Fundamental equation of state correlation for hexamethyldisiloxane based on experimental and molecular simulation data

M. Thol[a], F. H. Dubberke[b], G. Rutkai[b], T. Windmann[b], A. Köster[b], R. Span[a], J. Vrabec[b,*]

[a] *Lehrstuhl für Thermodynamik, Ruhr-Universität Bochum, 44801 Bochum, Germany*
[b] *Lehrstuhl für Thermodynamik und Energietechnik, Universität Paderborn, 33098 Paderborn, Germany*

Abstract

An empirical fundamental equation of state correlation in terms of the Helmholtz energy is presented for hexamethyldisiloxane. The relatively small amount of thermodynamic data that is available in the literature for this substances is considerably extended by speed of sound measurements and numerical results for Helmholtz energy derivatives from molecular modelling and simulation. The speed of sound apparatus employed in this work is based on the puls-echo technique and operates up to 150 MPa in the temperature range between 250 K and 600 K. The range of validity of the equation of state, based on laboratory data from literature and speed of sound data of this work, is from 270 K to 580 K and up to 130 MPa. Molecular simulation data are applied to extend the range of validity up to 1200 K and 600 MPa.

Keywords: thermodynamic properties, fundamental equation of state, molecular modelling and simulation, hexamethyldisiloxane

1. Introduction

In heat recovery systems, such as organic Rankine cycles (ORC), one important group of working fluids are siloxanes, which belong to the wider class of organo-silicone compounds. Among others, hexamethyldisiloxane (CAS No.: 107-46-0, $C_6H_{18}OSi_2$) appears to be a good candidate for becoming a widely employed working fluid for high temperature ORC processes. However, accurate thermodynamic data for siloxanes are a prerequisite for optimally designed processes.

Traditionally, thermodynamic properties obtained from experiments are summarized in different forms of empirical equations of state. Correlations of the fundamental equation of state (EOS) are particularly useful, because every thermodynamic equilibrium property can be expressed as a combination of derivatives of the thermodynamic potential in terms of which the EOS is explicit. However, a sufficient amount of thermodynamic data is a key factor when it comes to empirical EOS development.

For hexamethyldisiloxane a fundamental EOS was published by Colonna *et al.* [1] in 2006. Upon commission of our speed of sound measurement apparatus that is briefly described below, it was found

*Corresponding author: Jadran Vrabec, Warburger Str. 100, 33098 Paderborn, Germany, Tel.: +49-5251/60-2421, Fax: +49-5251/60-3522, Email: jadran.vrabec@upb.de

that this model yields unreliable data for this property. In fact, with up to 15 %, these deviations were so large that we decided to develop a molecular interaction model to independently corroborate our experimental findings.

Since 2006, the amount of experimental data that is available for hexamethyldisiloxane has expanded, particularly through the work of Abbas [2], but it is still rather poor; additional data sets were generated in the present work by means of speed of sound measurement and molecular modeling and simulation.

In principle, molecular simulation alone could provide any thermodynamic data at any state point and it is more cost and time efficient than laboratory measurements. However, its predictive capability is limited by the quality of the underlying molecular interaction model. Although molecular interaction models are usually adjusted only to a small amount of experimental data, it is generally accepted that they can provide reasonably good predictions for other state points and properties that were not considered during their optimization. However, consistently good inter- and extrapolation ability cannot be guaranteed. Our previous experience with several substances indicated that satisfactory performance still can be expected with respect to predicting various Helmholtz energy derivatives in the homogeneous fluid region, even if the molecular model was optimized exclusively to experimental vapor-liquid equilibrium data [3, 4, 5, 6, 7]. Nevertheless, due to the inherent uncertainty of molecular models, experimental data are still essential for EOS development.

Acoustic measurements allow for a fast and convenient access to the speed of sound. In case of fluids, such measurements contribute substantially to the development and parameterization of EOS [8], because accurate speed of sound data can efficiently be obtained over a large range of temperature and pressure. The common measuring principle for determining the speed of sound of liquids is the pulse-echo technique, which was introduced by Kortbeek *et al.* [9]. In this method, sound waves, emitted by an excited quartz crystal, propagate through a fluid over a known propagation distance, are reflected and travel back to the quartz crystal. The interference and correlation approaches are common for the pulse-echo technique for determining the propagation time of the wave signal. Here, the correlation approach was employed for the speed of sound measurement.

2. Speed of sound measurement

2.1. Measurement principle

Speed of sound measurements were carried out with the pulse-echo technique. By emitting a high frequency modulated burst signal with a piezoelectric quartz crystal, which was positioned in the fluid between two reflectors with different path lengths l_1 and l_2, where $l_1 < l_2$, the speed of sound was determined by the time measurement of the signal propagation through the fluid over a known distance [10, 11]. The speed of sound, neglecting dispersion and diffraction effects, is given by the ratio of the propagation distance and the propagation time

$$w = \frac{2(l_2 - l_1)}{\Delta t}. \tag{1}$$

The measurement of the propagation time difference Δt was based on the correlation method, which was also used by Ball and Trusler [12], combined with a signal enhancement by applying Fast Fourier Transformation (FFT) to the original echo signals [13, 14].

The quartz crystal was excited with a burst of 20 cycles, typically with a voltage of 10 V peak-to-peak. Both echoes were sampled, stored to a computer by an oscilloscope (Agilent, DSO1022A) and identified via a threshold. On the basis of the time intervals where the signals exceeded the specifed threshold, a significantly extended number of data points in the time interval Δt_e was marked around both echo maxima, starting at t_1 for the first echo and at t_2 for the second echo, cf. Fig. 1 (top).

Because the second echo is affected by greater attenuation due to the longer propagation distance than the first echo, the ratio of the maximum amplitudes of the first echo and the second echo had be determined. The resulting amplitude factor r, which depends on the fluid and its thermodynamic state, is required in the correlation approach to consider attenuation [12]. This was done here by multiplying the second echo, i.e. the signal data within Δt_e after t_2, with the amplitude factor to achieve the same maximum peak magnitude for both echoes, cf. Fig. 1 (center).

The correlation z overlays the signals of both echoes by

$$z(\Delta t) = \sqrt{\sum_{t_1}^{t_1+\Delta t_e} [x(t) \cdot rx(t+\Delta t)]^2}, \tag{2}$$

where $x(t)$ refers to the echo amplitude at the time t. The time at the maximum of z is the measured propagation time difference Δt, cf. Fig. 1 (bottom).

2.2. Measurement procedure

After filling siloxane into the cell, it was compressed to about 20 MPa by a hand-pump and an equilibration time of around 1 h was given to reach a constant pressure level. Each isotherm was studied from high pressure to vapor pressure, where the pressure was measured with a transducer (Honeywell TJE with an operating range from 0 to 70 MPa), which was calibrated with a dead weight tester (Degranges and Hout, 5201-S) and protected by a blowout disc.

The temperature was measured with a PT-100 thermometer (Rössel Messtechnik RM-type), which was mounted in the wall of the pressure cylinder next to the quartz and was calibrated with a standardized 25 Ω platinum thermometer (Rosemount 162 CE). Hence, the overall uncertainty of the temperature measurement results according to the error propagation law due the individual uncertainty contributions amounts to $u_\mathrm{T} = \pm 15$ mK.

For controlling the cell with a high accuracy over a wide temperature range, the thermostat was constructed with three nested copper shields. Each was monitored with respect to the temperature and equipped with one independently adjustable heater, which was controlled with a combination of a PID controller and an additional proportional (P) controller to quickly specify a constant temperature without overshooting.

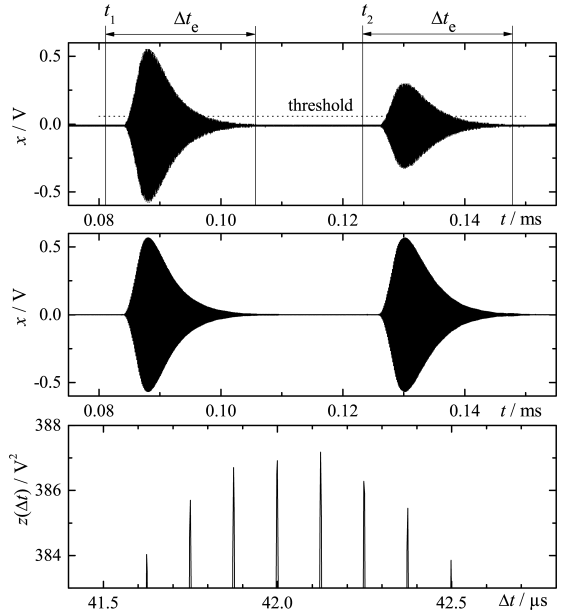

Figure 1: Steps of the correlation method. Top: First and second echo signals identified via a threshold. Center: Signal reconstructed by FFT where the amplitude of the second echo is the same as the amplitude of the first echo. Bottom: Correlation function $z(\Delta t)$ according to Eq. (2).

The referencing of the path length distance difference $\Delta l = l_2 - l_1$ was carried out with water, which is available at high purity and for which highly accurate speed of sound measurements are available over a wide range of states, see also [15]. The experimental speed of sound data were corrected by the diffraction correction by Harris [16], where significant dispersion effects are not expected for a resonance frequency of 8 MHz [17].

2.3. Results

Speed of sound measurements were carried out for a set of 12 isotherms in the temperature range from 365 K to 573 K up to 20 MPa, cf. Fig. 2. The siloxane was obtained from WACKER with a given purity of $\geq 99\%$ and was degassed before experimental measurements were carried out.

The uncertainty of the present measurements is larger for lower pressures mainly due to the uncertainty of the pressure sensor. The operating range of the pressure sensor was up to 70 MPa with an accuracy of $\pm 0.035\%$ of the full scale. Therefore the absolute uncertainty was 0.025 MPa. This uncertainty had the largest impact at high temperatures and low pressures. The overall speed of sound measurement uncertainty u_w is composed of the relevant contributions due to uncertainties of temperature and pressure measurements as well as the uncertainty of the referencing procedure.

According to the error propagation law, the total uncertainty was between 0.03 % and 0.3 %. The higher end of this uncertainty range is mainly caused by the fact that the relative uncertainty of the pressure measurement was significantly higher at low pressures, combined with the high isothermal

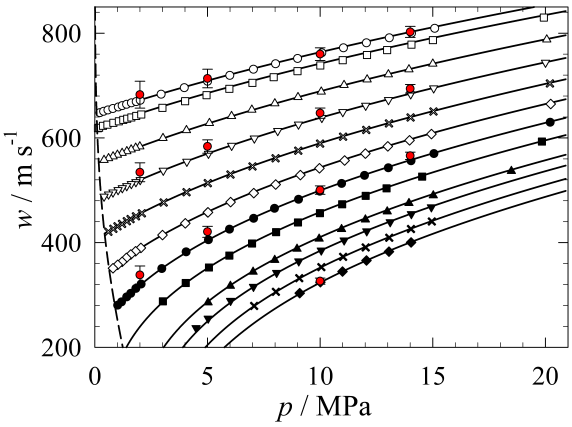

Figure 2: Speed of sound of hexamethyldisiloxane. Present experimental data: ○ 365 K, □ 373 K, △ 393 K, ▽ 413 K, × 433 K, ◇ 453 K, ● 473 K, ■ 493 K, ▲ 518 K, ▼ 533 K, × 553 K, ♦ 573 K; ○ (red) present simulation data; — present equation of state; - - vapor pressure curve.

compressibility of the fluid at such thermodynamic states. Numerical measurement data together with their uncertainties can be found in the Supplementary Material.

3. Molecular modeling and simulations

3.1. Molecular model

A molecular interaction model for hexamethyldisiloxane was developed here. It was validated with respect to experimental data or the respective correlations from literature, including saturated liquid density, vapor pressure, heat of vaporization, homogeneous liquid properties (density and speed of sound), second virial coefficient, and transport properties (thermal conductivity and shear viscosity).

The geometry of the model was determined by quantum chemical calculations using the software package GAMMES(US) [18] with the Hartree-Fock method and the 6-31G basis set. Three Lennard-Jones (LJ) sites and three point charges were placed on the silica (Si) and oxygen (O) atoms, while the six methyl groups (CH_3) were represented with LJ sites only, cf. Fig. 3. Its point charge magnitudes were specified such that they correspond to a dipole moment of $2.67 \cdot 10^{-30}$ Cm (a value taken from the DIPPR database [19]). The initial values of the LJ energy (ϵ) and size (σ) parameters of the CH_3 and O sites were adopted from Schnabel *et al.* [20] and Vrabec *et al.* [21], respectively. The LJ parameters of the Si sites were adjusted to experimental saturated liquid density and vapor pressure data. In a last step, all model parameters, including geometric structure and polarity, were fine-tuned with the reduced unit method [22]. The resulting model parameters are listed in Table 1.

3.2. Validation of the molecular model

To validate the present molecular interaction model, simulation results for vapor-liquid equilibria, homogeneous liquid density, speed of sound, second virial coefficient, and transport properties were

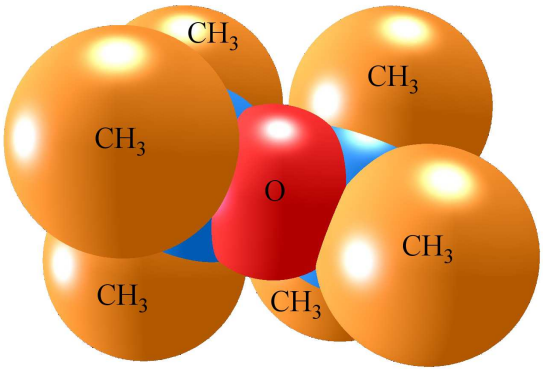

Figure 3: Present molecular interaction model for hexamethyldisiloxane. CH_3: methyl site, O: oxygen site, not labeled: silica site. Note that the sphere diameters correspond to the Lennard-Jones size parameters, which are depicted according to the molecular geometry scale.

compared with experimental data from literature and with correlations from the DIPPR database [19]. All simulation details and data are given in the Supplementary Material. The simulation data for vapor pressure, saturated liquid density, saturated vapor density, and enthalpy of vaporization are presented in absolute plots in the Supplementary Material. As discussed in section 4.3 in detail, for the vapor pressure relative deviations between the molecular simulation data and the present EOS are less than 4 % for all simulation points, except for the lowest temperature. Note that the experimental data scatter in this range, too. Experimental data for the saturated liquid density are available between 213 and 358 K only. The simulation data in this region are well within the scatter of the experimental data and the uncertainty of the DIPPR correlation [19]. The simulation results for the enthalpy of vaporization agree well with the experimental data over the whole temperature range from 287 K to 500 K. The relative deviations are throughout less than about 1.5 %, with the exception of the point at 495 K.

Simulation results for the homogeneous liquid density were compared to experimental data published by McLure *et al.* [23] and Abbas [2]. McLure *et al.* [23] provide data at 1 atm, Abbas [2] performed measurements over a wide temperature and pressure range. Fig. 4 shows the results of the comparison at temperatures from 303 to 427 K up to a pressure of 130 MPa. It can be seen that the agreement between simulation and experimental data is very satisfying. In general, the relative deviation is less than 0.2 %. For the three data points at 1 atm it is slightly higher.

The speed of sound w in the liquid state was calculated by simulation, taking the ideal gas contribution of the present EOS into account (see section 4.1). These results were compared with the experimental data generated in the present work. As can be seen in Fig. 2, the simulation results are in line with the experimental data points at the four investigated isotherms 365, 413, 473, and 573 K up to a pressure of 14 MPa. Nearly all simulation points agree with the experiment within their statistical uncertainties.

Table 1: Parameters of the present molecular interaction model for hexamethyldisiloxane. Lennard-Jones sites are denoted by the modeled atoms or atomic groups. Electrostatic sites are denoted by point charge magnitudes q. Coordinates are given with respect to the center of mass in a principal axes system.

interaction site	x	y	z	σ	ϵ/k_B	q
	Å	Å	Å	Å	K	e
CH_3	-2.2796	-0.8698	-0.3545	3.8144	121.3515	
CH_3	-2.2150	1.2764	1.8825	3.8144	121.3515	
CH_3	0.5674	0.7717	-2.5502	3.8144	121.3515	
Si	-1.2334	-0.0730	1.0059	3.5133	15.1500	0.1458
O	0.1238	0.6680	0.3350	3.1180	43.6148	-0.2916
Si	1.2923	0.3890	-0.8475	3.5133	15.1500	0.1458
CH_3	-0.6830	-1.3930	2.2409	3.8144	121.3515	
CH_3	1.8613	-1.4145	-0.7878	3.8144	121.3515	
CH_3	2.7335	1.5447	-0.4734	3.8144	121.3515	

The second virial coefficient was predicted over a temperature range from 220 K to 1500 K by evaluating Mayer's f-function. This approach was described e.g. by Eckl *et al.* [24]. The present results are shown in section 4.5, where the mean absolute deviation over the whole considered temperature range is below 0.44 dm^3/mol.

Thermal conductivity and shear viscosity of liquid hexamethyldisiloxane were obtained by equilibrium molecular dynamics simulations following the Green-Kubo formalism, cf. Guevara-Carrion *et*

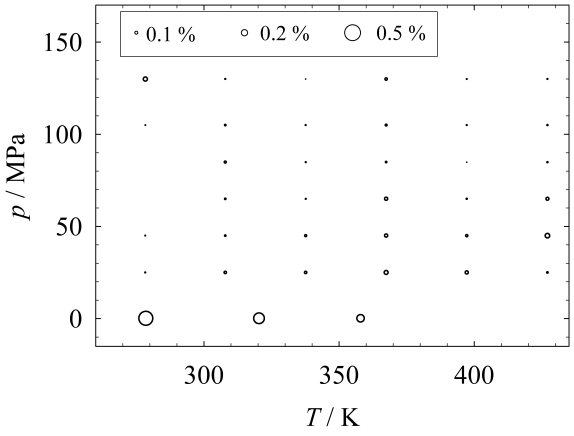

Figure 4: Density in the homogeneous liquid region of hexamethyldisiloxane. Relative deviations between present simulation data and experimental data by Abbas [2] and McLure *et al.* [23] ($\delta z = (z_{\mathrm{sim}} - z_{\mathrm{exp}})/z_{\mathrm{exp}}$). The size of the bubbles indicates the magnitude of the relative deviation.

al. [25]. Fig. 5 shows the simulation results in comparison with experimental data from the literature and a correlation from the DIPPR database [19]. For the thermal conductivity, simulations were carried out at $p = 10$ MPa, cf. Fig. 5 (top). The simulations agree with the experimental data by Abbas [2] mostly within their statistical uncertainties. At 500 K, there is some deviation. The shear viscosity experimental data at 1 atm, published by Abbas [2], Hurd [26], and Wilcock [27], were used for comparison. The shear viscosity from simulation is about 0.1 Pa s below the experimental data in the entire temperature range from 280 to 350 K, cf. Fig. 5 (bottom). The mean relative deviation of the simulation data with respect to the correlation from the DIPPR database [19] is about 18 %.

3.3. Large scale thermodynamic data generation

In principle, once a molecular interaction model is available, any thermodynamic information can be obtained from molecular simulation. However, the generation of a data set that contains as much non-redundant thermodynamic information as possible may look cumbersome in practice, because standard textbook approaches in the molecular simulation literature imply that specific statistical mechanical ensembles are required for particular thermodynamic properties. It is true that certain properties

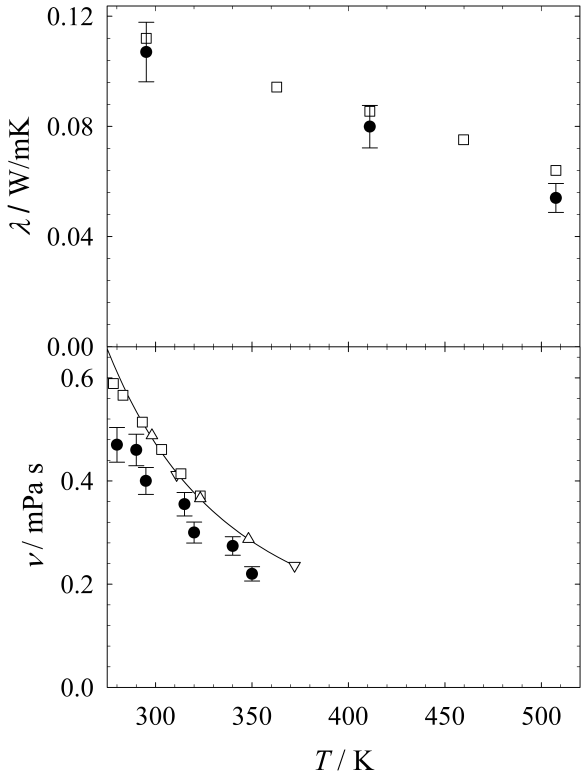

Figure 5: Thermal conductivity at 10 MPa (top) and shear viscosity at 1 atm (bottom) of hexamethyldisiloxane: • present simulation data; □ experimental data by Abbas [2], △ Hurd [26], and ▽ Wilcock [27]; — correlation of experimental data from the DIPPR database [19].

have simpler statistical analogs in certain ensembles and may be difficult to derive in others, but it is nevertheless possible. The statistical mechanical formalism proposed by Lustig [28, 29] was designed to provide an arbitrary number of Helmholtz energy derivatives

$$A^{\mathrm{r}}_{xy} = \tau^x \delta^y \frac{\partial^{x+y} \alpha^{\mathrm{r}}(\tau,\delta)}{\partial \tau^x \partial \delta^y} = (1/T)^x \rho^y \frac{\partial^{x+y} \alpha^{\mathrm{r}}(T,\rho)}{\partial (1/T)^x \partial \rho^y}, \tag{3}$$

from a single molecular simulation run for a given state point. In Eq. (3) α is the reduced Helmholtz energy, T the temperature, ρ the density, R the molar gas constant, $\tau = T_{\mathrm{c}}/T$ the inverse reduced temperature, and $\delta = \rho/\rho_{\mathrm{c}}$ the reduced density, in which T_{c} is the critical temperature and ρ_{c} the critical density. α is commonly divided into an ideal (superscript "o") and residual (superscript "r") contribution

$$\alpha(\tau,\delta) = \frac{a^{\mathrm{o}}(T,\rho) + a^{\mathrm{r}}(T,\rho)}{RT} = \alpha^{\mathrm{o}}(\tau,\delta) + \alpha^{\mathrm{r}}(\tau,\delta), \tag{4}$$

where a is the molar Helmholtz energy. The ideal contribution $\alpha^{\mathrm{o}}(T,\rho) = \alpha^{\mathrm{o}}(T) + \alpha^{\mathrm{o}}(\rho)$ corresponds to the value of $\alpha(T,\rho)$ when no intermolecular interactions are at work [8]. The density dependence of $\alpha^{\mathrm{o}}(T,\rho)$ is known from the ideal gas law and it is $\alpha^{\mathrm{o}}(\rho) = \ln(\rho/\rho_{\mathrm{ref}})$. The exclusively temperature dependent ideal part $\alpha^{\mathrm{o}}(T)$ has a non-trivial temperature dependence and it is is often determined by spectroscopy or *ab initio* calculations. Although molecular interaction models with internal degrees of freedom may describe $\alpha^{\mathrm{o}}(T)$ accurately, the residual contribution $\alpha^{\mathrm{r}}(T,\rho) = \alpha(T,\rho) - \alpha^{\mathrm{o}}(T,\rho)$ is typically the target of molecular simulation.

The formalism proposed by Lustig is an implemented feature of our molecular simulation tool *ms*2 [30, 31] that yields up to eight derivatives of the residual Helmholtz energy. With this method, the analytical derivatives of Eq. (3) can be directly fitted to A^{r}_{xy} simulation results, unlike usual thermodynamic properties, such as pressure p, isochoric heat capacity c_v, isobaric heat capacity c_p, and speed of sound w

$$\frac{p}{\rho RT} = 1 + A^{\mathrm{r}}_{01}, \tag{5}$$

$$\frac{c_v}{R} = -(A^{\mathrm{o}}_{20} + A^{\mathrm{r}}_{20}), \tag{6}$$

$$\frac{c_p}{R} = -(A^{\mathrm{o}}_{20} + A^{\mathrm{r}}_{20}) + \frac{(1 + A^{\mathrm{r}}_{01} - A^{\mathrm{r}}_{11})^2}{1 + 2A^{\mathrm{r}}_{01} + A^{\mathrm{r}}_{02}}, \tag{7}$$

$$\frac{Mw^2}{RT} = 1 + 2A^{\mathrm{r}}_{01} + A^{\mathrm{r}}_{02} - \frac{(1 + A^{\mathrm{r}}_{01} - A^{\mathrm{r}}_{11})^2}{A^{\mathrm{o}}_{20} + A^{\mathrm{r}}_{20}}, \tag{8}$$

that are linear or non-linear functions of A_{xy}. This approach is a convenient route to obtain an arbitrary number of independent thermodynamic properties, and its contribution to support EOS development was recently shown [3, 4, 5, 6, 7]. The large scale molecular simulation data set of the present work contains five derivatives A^{r}_{10}, A^{r}_{01}, A^{r}_{20}, A^{r}_{11}, and A^{r}_{02} as well as A^{r}_{00} at 194 state points that are

well distributed in the homogeneous fluid region. At each state point 864 particles were sufficiently equilibrated and then sampled for 2 million production cycles with NVT Monte Carlo simulations [32]. Electrostatic long-range corrections were approximated by the reaction field method [33]. The reduced residual Helmholtz energy A_{00}^{r} was determined by Widom's test particle insertion [34]. A discussion of these data is given in section 4.6, their numerical values can be found in the Supplementary Material.

4. Fundamental equation of state correlation

In this section, an EOS for hexamethyldisiloxane is presented. Comparisons are made to experimental as well as molecular simulation data, and the physical and extrapolation behavior is analyzed. The present EOS for hexamethyldisiloxane is written in terms of the reduced Helmholtz energy as a function of temperature and density. Because this is a thermodynamic potential, every other equilibrium thermodynamic property can be obtained by differentiating Eqs. (10) and (11) analytically and combining the results. Examples, e.g. for the pressure, are given in Eqs. (5) to (8).

4.1. Ideal gas contribution

The exclusively temperature dependent ideal contribution $\alpha^{\mathrm{o}}(\tau)$ of the reduced Helmholtz energy $\alpha(\tau,\delta)$ was derived from a c_p^{o} equation

$$\frac{c_p^{\mathrm{o}}}{R} = n_0 + \sum_{i=1}^{I_{\mathrm{Pol}}} n_i \tau^{t_i} + \sum_{i=I_{\mathrm{Pol}}+1}^{I_{\mathrm{Pol}}+I_{\mathrm{PE}}} m_i \left(\frac{\theta_i}{T}\right)^2 \frac{\exp\left(\theta_i/T\right)}{\left(\exp\left(\theta_i/T\right)-1\right)^2}. \tag{9}$$

For the application to a fundamental EOS in terms of the Helmholtz energy, this equation has to be integrated twice with respect to τ

$$\alpha^{\mathrm{o}}\left(\tau,\delta\right) = c^{\mathrm{II}} + c^{\mathrm{I}}\tau + c_0 \ln\left(\tau\right) + \sum_{i=1}^{I_{\mathrm{Pol}}} c_i \tau^{t_i} + \sum_{i=I_{\mathrm{Pol}}+1}^{I_{\mathrm{Pol}}+I_{\mathrm{PE}}} m_i \ln\left(1-\exp\left(-\theta_i/T_{\mathrm{c}}\,\tau\right)\right) + \ln\left(\delta\right). \tag{10}$$

The integration constants c^{I} and c^{II} can be chosen arbitrarily. However, the most common reference state is the normal boiling point (NBP). Here, the temperature and density of the saturated liquid at the reference pressure $p_0 = 1$ atm have to be determined. At this state point, the default values of the corresponding reference entropy $s_0(T_{\mathrm{NBP}}, p_0 = 1\ \mathrm{atm})$ and enthalpy $h_0(T_{\mathrm{NBP}}, p_0 = 1\ \mathrm{atm})$ are set to be zero. Therefore, c^{I} and c^{II} depend on the residual part of the recent equation of state.

In general, c_p^{o} equations are correlated to data for the isobaric heat capacity of the ideal gas. These data can be determined from spectroscopy, statistical mechanics, or extrapolation from gaseous speed of sound or isobaric heat capacity measurements. Spectroscopic data are very difficult to analyze for complex molecules. Therefore, they can rarely be used to set up equations of state. When extrapolating ideal gas heat capacities from experimental speed of sound or isobaric heat capacity data, highly accurate measurements are mandatory. Thus, such data are only available for well investigated fluids. Therefore, most data were determined by means of statistical mechanics. Depending on the complexity of the molecule, these data can be associated with high uncertainties so that they have to be treated carefully.

Table 2: Parameters of the ideal contribution of the present equation of state of hexamethyldisiloxane according to Eq. (10).

i	m_i	θ_i/K
1	18.59	20
2	29.58	1400
3	19.74	3600
4	4.87	6300
c_0	3.0	
c^{I}	-10.431499	
c^{II}	72.110754	

When developing a c_p^{o} equation, some boundary conditions have to be kept in mind. The functional form of Eq. (9) is physically based and the contributions of molecular translation and rotation are combined in the temperature independent part n_0. For s molecule like hexamethyldisiloxane, it can be assumed that the degrees of freedom of both contributions are fully excited also for very low temperatures. Therefore, $n_0 = 4$, corresponding to three degrees of freedom for translation and three degrees of freedom for rotation. The temperature dependent contribution of the molecular vibrations was modeled by the Planck-Einstein terms. For high temperatures, it has to be ensured that the ideal gas heat capacity approaches a maximum value related to fully excited degrees of freedom considering all contributions, i.e. translation, rotation, and vibration. Since it is too complex to express these contributions on a strictly physical basis, the Planck-Einstein terms were treated empirically. The ideal contribution of the present EOS for hexamethyldisiloxane thus consists of four Planck-Einstein terms and the corresponding parameters are given in Table 2. In Fig. 6, the representation of the isobaric heat capacity of the ideal hexamethyldisiloxane gas is illustrated. The upper part of that figure shows the absolute trend of c_p^{o}/T as a function of temperature. The present equation has a correct extrapolation behavior for low temperatures, i.e. $c_p^{\mathrm{o}}(T \to 0\ \mathrm{K}) = 4R$. For high temperatures, an asymptotic behavior of the equation can be observed. Colonna *et al.* [1] have chosen a simple polynomial approach for fast calculations. This can be helpful when insufficient data are available for the correlation. However, these polynomial terms have to be used carefully because it is easily possible to compromize the extrapolation behavior. As a result from the chosen functional form, the transition of the equation of Colonna *et al.* [1] to very low temperatures yields a value of $6.3R$ and for increasing temperatures the ideal gas heat capacity decreases.

In Fig. 6 (bottom), relative deviations of literature data from the present EOS are shown. Only three different datasets are available, where Mosin and Mikhailov [35] derived their data from statistical mechanics. Since no information is given on the accuracy of these data, they were not considered in the development of the present c_p^{o} equation. The data of Scott *et al.* [36] were gained from low

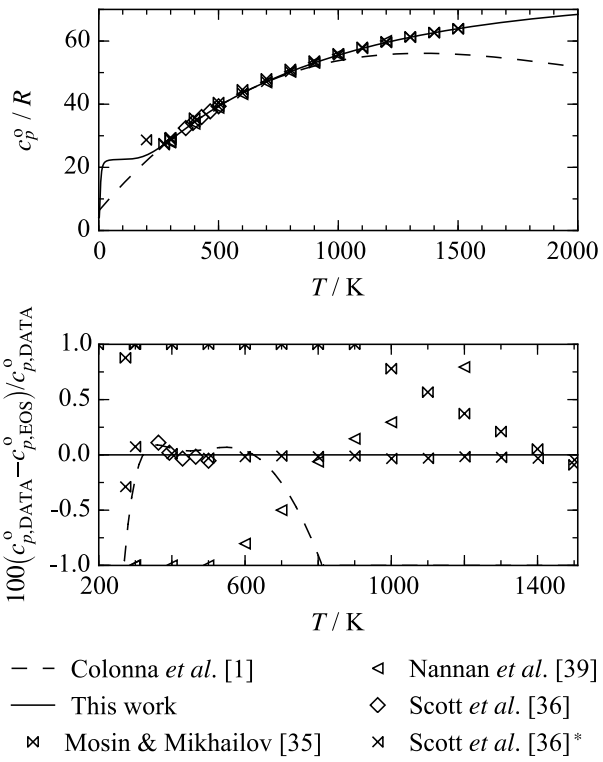

Figure 6: Isobaric heat capacity of the ideal gas of hexamethyldisiloxane.

temperature calometric measurements. Due to limitations of their apparatus, the temperature range was only 360 to 500 K. Additionally, they used results from investigations on the barrier restricting internal rotation around the Si-O bond to determine the ideal gas heat capacity theoretically, which are in good agreement with their measurements. Therefore, the low temperature region ($T < 500$ K) of the present equation was correlated to the experimental results of Scott *et al.* [36], and higher temperatures were modeled with the help of their theoretical results. For $T < 300$ K, the ideal gas heat capacity is reproduced within 0.1 %, which is also claimed to be the uncertainty of the present equation. For lower temperatures deviations increase.

When Colonna *et al.* [1] developed their EOS in 2006, no information on the ideal gas heat capacity was available. Therefore, they applied the Harrison-Seaton zeroth order contribution method [37] to gain information on this property. Unfortunately, the method yields results with 25 % uncertainty [19], which is too large for accurate EOS. However, this was the only group contribution method applicable to siloxanes, because it is the only one providing information on Si-O bonds. Poling *et al.* [38] state the same findings, which led to further investigations on the ideal gas heat capacity of siloxanes by Nannan *et al.* [39]. They made *ab initio* calculations, which were based on information about hexamethyldisiloxane from literature, and were then transferred to several other siloxanes. Unfortunately, these results were not compared to their experimental results for octamethylcyclotetrasiloxane so that it is not possible to assess the accuracy of their *ab initio* calculations. In a publication that reports a conclusion of

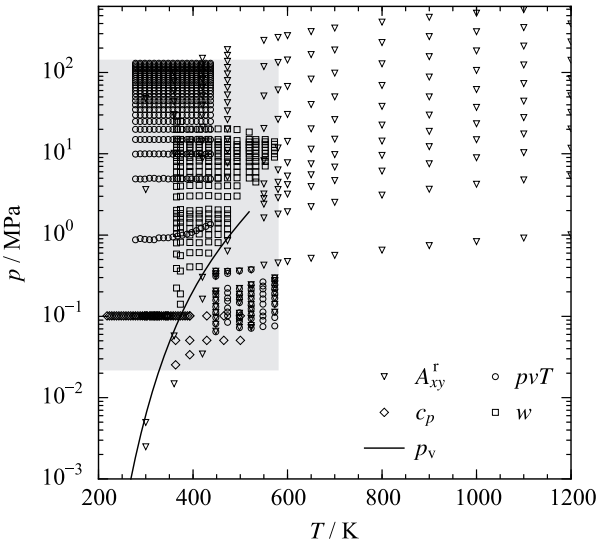

Figure 7: Data in the homogeneous region of hexamethyldisiloxane. The grey area depicts the region where experimental data are available: $T_{\max} = 580$ K and $p_{\max} = 130$ MPa. Helmholtz energy derivatives from molecular simulation extend this region up to $T_{\max} = 1200$ K and $p_{\max} = 600$ MPa.

their investigations on more accurate ideal gas heat capacities of siloxanes, they claim that the HF/6-31G(d) method is the most accurate one. This method yields an ideal gas isobaric heat capacity of $c_p^\mathrm{o} = 503\ \mathrm{J \cdot mol^{-1} \cdot K^{-1}}$ at $T = 500$ K, which is the same value as their experiment at $T = 495$ K. Therefore, these data are assumed to be less accurate than the data of Scott *et al.* [36] and were only used for comparison here.

4.2. Residual contribution

The residual contribution consists of polynomial, exponential, and Gaussian bell-shaped terms

$$\begin{aligned}\alpha^\mathrm{r}(\tau,\delta) &= \alpha^\mathrm{r}_\mathrm{Pol}(\tau,\delta) + \alpha^\mathrm{r}_\mathrm{Exp}(\tau,\delta) + \alpha^\mathrm{r}_\mathrm{GBS}(\tau,\delta) \\ &= \sum_{i=1}^{I_\mathrm{Pol}} n_i \delta^{d_i} \tau^{t_i} + \sum_{i=I_\mathrm{Pol}+1}^{I_\mathrm{Pol}+I_\mathrm{Exp}} n_i \delta^{d_i} \tau^{t_i} \exp\left(-l_i \delta^{p_i}\right) \\ &+ \sum_{i=I_\mathrm{Pol}+I_\mathrm{Exp}+1}^{I_\mathrm{Pol}+I_\mathrm{Exp}+I_\mathrm{GBS}} n_i \delta^{d_i} \tau^{t_i} \exp\left(-\eta_i(\delta-\varepsilon_i)^2 - \beta_i(\tau-\gamma_i)^2\right).\end{aligned} \tag{11}$$

Polynomial and exponential terms are generally sufficient to accurately describe the whole fluid region, except for critical states. The Gaussian bell-shaped terms [40], which were first applied to Helmholtz EOS by Setzmann and Wagner [41] in 1991, are used for a more accurate description of the critical region. Furthermore, they allow for the development of EOS, which can reproduce data within their experimental uncertainty with a much lower number of terms as before.

The residual contribution of the present EOS consists of five polynomial, five exponential, and eight Gaussian bell-shaped terms. The corresponding parameters are listed in Table 3. These parameters

Table 3: Parameters of the residual contribution of the present equation of state of hexamethyldisiloxane according to Eq. (11), where $l_i = 1$.

i	n_i	t_i	d_i	p_i	η_i	β_i	γ_i	ϵ_i
1	$0.5063651 \cdot 10^{-1}$	1.000	4	-				
2	$0.8604724 \cdot 10^{+1}$	0.346	1	-				
3	$-0.9179684 \cdot 10^{+1}$	0.460	1	-				
4	$-0.1146325 \cdot 10^{+1}$	1.010	2	-				
5	$0.4878559 \cdot 10^{+0}$	0.590	3	-				
6	$-0.2434088 \cdot 10^{+1}$	2.600	1	2				
7	$-0.1621326 \cdot 10^{+1}$	3.330	3	2				
8	$0.6239872 \cdot 10^{+0}$	0.750	2	1				
9	$-0.2306057 \cdot 10^{+1}$	2.950	2	2				
10	$-0.5555096 \cdot 10^{-1}$	0.930	7	1				
11	$0.9385015 \cdot 10^{+1}$	1.330	1	-	1.0334	0.4707	1.7754	0.8927
12	$-0.2493508 \cdot 10^{+1}$	1.680	1	-	1.5440	0.3200	0.6920	0.5957
13	$-0.3308032 \cdot 10^{+1}$	1.700	3	-	1.1130	0.4040	1.2420	0.5590
14	$-0.1885803 \cdot 10^{+0}$	3.080	3	-	1.1130	0.5170	0.4210	1.0560
15	$-0.9883865 \cdot 10^{-1}$	5.410	1	-	1.1100	0.4320	0.4060	1.3000
16	$0.1111090 \cdot 10^{+0}$	1.400	2	-	7.2000	7.2000	0.1630	0.1060
17	$0.1061928 \cdot 10^{+0}$	1.100	3	-	1.4500	1.2000	0.7950	0.1810
18	$-0.1452454 \cdot 10^{-1}$	5.300	1	-	4.7300	35.8000	0.8800	0.5250

Table 4: Critical parameters from literature, where the critical density was not measured, but estimated from theoretical models.

Author	T_c	p_c	ρ_c
	K	MPa	mol·dm^{-3}
Dickinson *et al.* [48]	518.8	1.91	1.715
McLure and Dickinson [45]	518.7	1.92	
McLure and Neville [49]			1.589
Nikitin *et al.* [50]	519	1.92	
Young [51]	516.6	1.91	1.745
Young [52]	516.6	1.91	1.744
This work	518.7	1.93	1.653

were determined by non-linear fitting techniques, which were also used to set up other modern EOS, e.g. R-125 [42], propane [43], or propylene [44]. Tables 5 and 6 list all data sources, indicating which data were considered in the present fitting routine. Their selection is discussed in detail below. The available dataset is presented in Fig. 7. The shaded area marks the region that is covered by experimental measurements ($T = 220$ K to 570 K, $p_{max} = 130$ MPa). Most are homogeneous liquid density and speed of sound data. The experimental dataset was supplemented here by Helmholtz energy derivatives from molecular simulation. In this way, the range of validity of the present equation of state was extended to a maximum temperature of $T_{max} = 1200$ K and a maximum pressure of $p_{max} = 600$ MPa. The critical temperature was constraint to the value of McLure and Dickinson [45] ($T_c = 518.7$ K), which is in close agreement with the other literature values (cf. Table 4). The critical density $\rho_c = 1.653$ mol·dm^{-3} and the critical pressure $p_c = 1.9311$ MPa were determined during the present fitting procedure. The critical pressure agrees well with the literature values, whereas the critical density differs by up to 5.5 %. However, none of the critical density values given in the literature are measurements, they were rather estimated from theoretical models. The triple point temperature $T_{tp} = 204.93$ K was taken from Scott *et al.* [36]. The corresponding liquid triple point density $\rho_{tp,liq} = 5.266$ mol·dm^{-3} was determined by extrapolating the saturated liquid line to the triple point temperature. Furthermore, the gas constant $R = 8.3144621$ J·mol^{-1} · K^{-1} [46] and the molecular weight $M = 162.3768$ g·mol^{-1} [47] were applied.

4.3. Assessment of vapor-liquid equilibrium properties

Relative deviations of experimental vapor pressure data from the present equation of state are shown in Fig. 8. Additionally, the corresponding average absolute relative deviations are listed in Table 5. Relative deviations were calculated by

$$\Delta X = 100 \left(\frac{X_{\mathrm{DATA}} - X_{\mathrm{EOS}}}{X_{\mathrm{DATA}}} \right). \tag{12}$$

Based on this definition, the average absolute relative deviation is defined as

$$\mathrm{AAD} = \frac{1}{N}\sum_{i=1}^{N}\left|\Delta X_i\right|. \tag{13}$$

Vapor-liquid equilibrium data were separated into three temperature ranges: low temperature (LT: $T/T_\mathrm{c} \leq 0.6$), medium temperature (MT: $0.6 \leq T/T_\mathrm{c} \leq 0.98$), and high temperature (HT: $T/T_\mathrm{c} > 0.98$). All other properties were classified into gas, liquid, critical region ($0.98 \leq T/T_\mathrm{c} \leq 1.1$ and $0.7 \leq \rho/\rho_\mathrm{c} \leq 1.4$), and supercritical region. The latter was further divided into low density (LD: $\rho/\rho_\mathrm{c} \leq 0.6$), medium density (MD: $0.6 \leq \rho/\rho_\mathrm{c} \leq 1.5$), and high density (HD: $\rho/\rho_\mathrm{c} > 1.5$). In the figures, the equation of state of Colonna *et al.* [1] and the ancillary equations of the DIPPR [19] and TDE [53] databases are plotted for comparison.

The large number of authors in Table 5 may lead to the impression that the vapor pressure was very well investigated. However, in many references only a single data point is reported. Most of these publications focused on measurements of mixture properties with hexamethyldisiloxane as an involved component. For verification of the sample purity, the normal boiling point was reported. These values differ by more than 1 % from each other so that they were not useful for the development of the present EOS. When excluding these data from the dataset, measurements by six different authors remain, which are mostly located between $T = 300$ K and 400 K.

Abbas [2] reports a comprehensive investigation on thermodynamic properties of hexamethyldisiloxane for a sample purity of 99.7 %. The vapor pressure was measured with a comparative ebulliometer, which requires a very well known reference fluid with a high purification grade. No information is given on the reference fluid in her thesis. Since she is calling her apparatus a "Scott-ebulliometer", it is assumed here that she was using water as a reference fluid as recommended in the original paper describing the apparatus [81]. This method is known to be very accurate, but Abbas' [2] data exhibit a systematic negative offset when comparing to the present EOS and other literature data, e.g. Scott *et al.* [36] or Flaningam [57]. For low temperatures the data by Abbas [2] scatter significantly, which could be due the choice of the reference fluid. Because water can easily be superheated for vapor pressures of $p < 0.0027$ MPa, other reference fluids should be chosen for the low temperature region. The specified uncertainties of $\Delta_p = 0.0005 \cdot p_\mathrm{v} + 10$ Pa and $\Delta_T = 0.05$ K yield a combined uncertainty of 0.4 % - 1.5 % for a coverage factor $k = 2$. No information is given how these uncertainties were ascertained and the sample purity was not considered.

The vapor pressure measurements of Scott *et al.* [36] and Flaningam [57] agree with each other within approximately 0.5 %. Scott *et al.* [36] report a very detailed description of their sample preparation. The sample purity of 99.996 % was verified by calorimetric studies of the melting point as a function of fraction melted. Similar to Abbas [2], Scott *et al.* [36] used a comparative ebulliometer for their measurements. As reference, water was used for high temperatures only, benzene was applied in case of low temperatures. This procedure yields consistent vapor pressure data over the whole temperature range. The measurements of Dickinson *et al.* [48] confirm the data of Scott *et al.* [36]

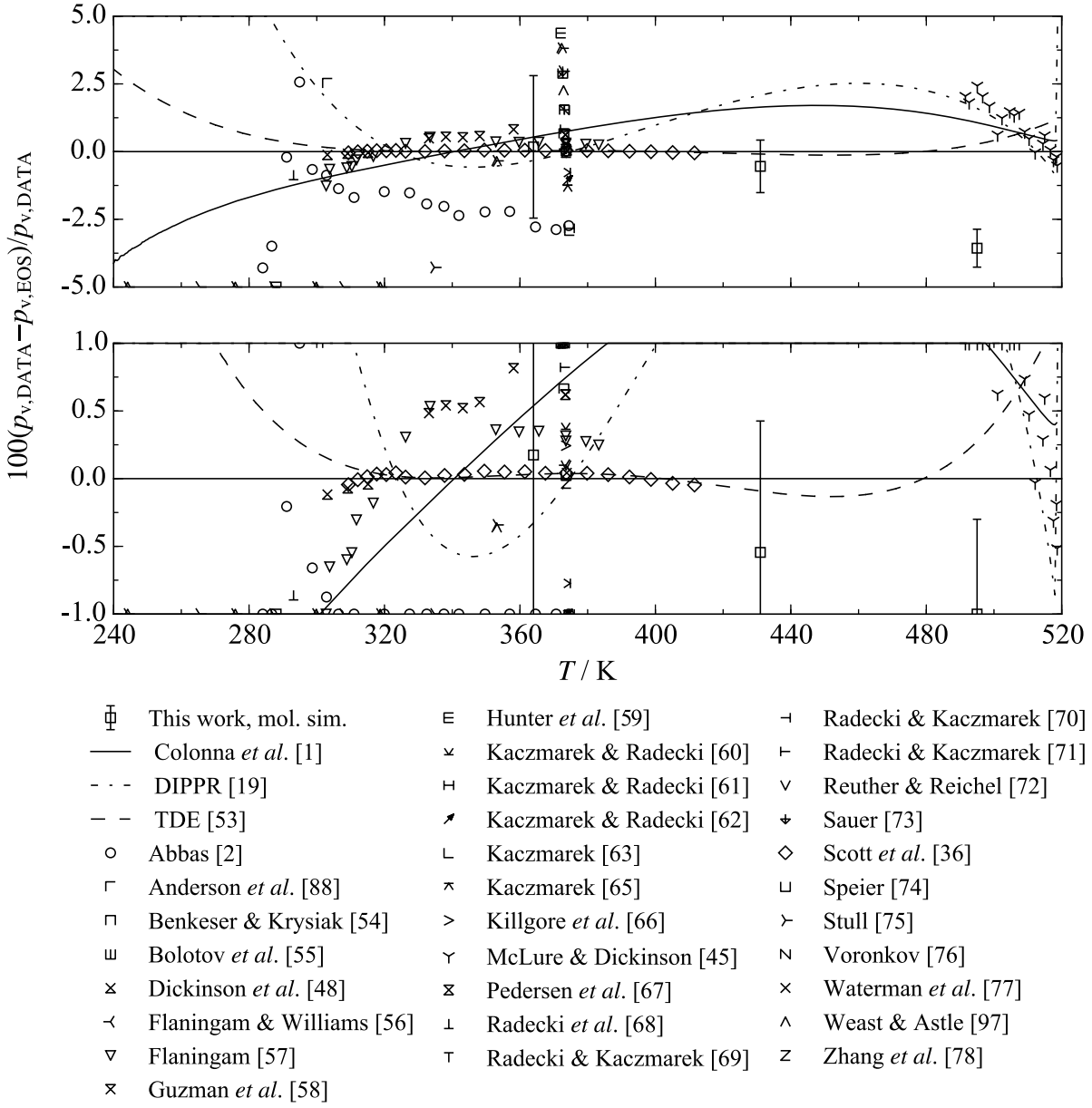

Figure 8: Relative deviations of experimental vapor pressure data from the present equation of state for hexamethyldisiloxane.

Table 5: Average absolute relative deviations of experimental vapor pressure and saturated liquid density data from the present equation of state for hexamethyldisiloxane. All temperatures were adapted to the ITS-90 scale. Datasets, which were applied to the fit, are marked with an asterisk.

	No. of	Temperature	Average absolute relative deviations (AAD) / %			
Authors	**data**	**range**	**LT**	**MT**	**HT**	**overall**
Vapor pressure p_v						
Abbas [2]	18	284 - 375	1.894	2.214	-	2.072
Benkeser & Krysiak [54]	1	372 - 373	-	2.966	-	2.966
Bolotov *et al.* [55]	1	373 - 374	-	1.541	-	1.541
Dickinson *et al.* [48]	3	303 - 316	0.093	0.041	-	0.076
Flaningam & Williams [56]	1	373 - 374	-	0.023	-	0.023
Flaningam [57]	15	302 - 384	0.765	0.318	-	0.437
Guzman *et al.* [58]	6	333 - 374	-	0.589	-	0.589
Hunter *et al.* [59]	1	372 - 373	-	2.966	-	2.966
Kaczmarek & Radecki [60]	1	374 - 375	-	2.833	-	2.833
Kaczmarek & Radecki [61]	1	374 - 375	-	1.066	-	1.066
Kaczmarek & Radecki [62]	1	374 - 375	-	1.066	-	1.066
Kaczmarek [63]	1	373 - 374	-	0.099	-	0.099
Kaczmarek [64]	1	373 - 374	-	0.774	-	0.774
Kaczmarek [65]	1	374 - 375	-	2.912	-	2.912
Killgore *et al.* [66]	1	372 - 373	-	0.663	-	0.663
McLure & Dickinson [45]*	19	491 - 519	-	1.615	0.38	1.030
Pedersen *et al.* [67]	1	373 - 374	-	0.620	-	0.620
Radecki *et al.* [68]	2	293 - 375	0.860	1.359	-	1.110
Radecki & Kaczmarek [69]	2	373 - 374	-	1.541	-	1.541
Radecki & Kaczmarek [70]	1	373 - 374	-	1.541	-	1.541
Radecki & Kaczmarek [71]	1	373 - 374	-	0.822	-	0.822
Reuther & Reichel [72]	1	373 - 374	-	0.099	-	0.099
Sauer [73]	1	373 - 374	-	0.243	-	0.243
Scott *et al.* [36]*	21	309 - 412	0.044	0.030	-	0.031
Speier [74]	1	372 - 373	-	4.376	-	4.376
Stull [75]	10	244 - 373	18.34	4.428	-	12.78
Voronkov [76]	1	373 - 374	-	0.388	-	0.388
Waterman *et al.* [77]	1	373 - 374	-	0.043	-	0.043
Zhang *et al.* [78]	1	373 - 374	-	0.035	-	0.035
Saturated liquid density ρ'						
Gubareva [79]	10	273 - 354	0.249	0.085	-	0.167
Guzman *et al.* [58]	5	333 - 359	-	1.335	-	1.335
Mills & MacKenzie [80]	2	293 - 303	0.109	-	-	0.109

at low temperatures. The three state points between $T = 303$ K and 315 K are reproduced with an $AAD = 0.076$ %. At $T = 373$ K, the most recent measurement of the normal boiling point by Zhang *et al.* [78] from 2011 also agrees very well with the data by Scott *et al.* [36]. Therefore, the present equation was fitted to the data of Scott *et al.* [36]. These data are reproduced within 0.06 % ($AAD = 0.031$ %), which is well within the expected uncertainty. Flaningam [57] carried out his measurements with a sample purity of 99.9 % using an ebulliometer as proposed by Stull [82]. In comparison to the comparative ebulliometer, the usage of a capacitive pressure sensor enables for the investigation of the low temperature regime without any modification of the apparatus. In his publication, he verified his apparatus with test measurements on water, methylcyclohexane, and diphenyl ether. However, except for water, these fluids are not practical for test measurements because they are not well investigated. The average pressure error of 0.07 % is not expressed in absolute values, which falsifies the results by opposite algebraic signs. Nonetheless, most of the data are reproduced within 0.5 % ($AAD = 0.437$ %).

The data by Stull *et al.* [75] are presented in a paper together with several hundred additional fluids. Thus, they were not measured, but collected from literature. Compared to the present EOS and other literature sources, these data show huge deviations ($AAD = 12.78$ %) and were thus not taken into account. The vapor pressure measurements of Guzman *et al.* [58] exhibit a systematic positive offset when comparing to the present EOS or the data of Scott *et al.* [36]. In their publication, the procedure of sample preparation is described in detail. However, they do not give the value of their sample purity. The only hint is a comparison of the NBP to the value published by Radecki and Kaczmarek [71]. Because their value already differs by 0.82 % from the present EOS, this confirmation is questionable and the positive deviation of the vapor pressure data of Guzman *et al.* [58] from the present EOS is reasonable.

Finally, there is one dataset of McLure and Dickinson [45] in the high temperature region ($T = 491$ K to 519 K). Because there are no other data available in this region, they cannot be compared to other measurements. Moreover, the lack of data between $T = 412$ K and 491 K prohibits a reliable transition from the low temperature region to the data of McLure and Dickinson [45]. Therefore, the accuracy of these data can only be evaluated with the information given in the corresponding publication and by comparison to the present EOS. They state a sample purity of 99.99 %, which was determined with gas chromatography. The experiment was carried out with Pyrex tubes [83] and the temperature was monitored with a thermo couple (type K), which is a quite inaccurate device, if it is not calibrated very carefully. However, the choice of calibrating the thermo couple to the critical points of hexane, heptane, octane, and nonane is questionable. All of these hydrocarbons are not well investigated and are barely available with a sufficient purity from common manufacturers (e.g. Sigma-Aldrich Co. LLC [84], Merck Millipore Corporation [85], or Alfa Aesar GmbH & Co. KG [86]). This is affirmed by the quite low sample purities of heptane (99.5 %) and octane (99 %) [83], which were used for calibration. Furthermore, the critical temperatures of hexane ($T_c = 507.4$ K) and octane ($T_c = 568.7$ K) [45] differ from those of the EOS of Lemmon and Span [87], which are the most accurate models in the literature

for these fluids (hexane: T_c = 507.82 K, octane: T_c = 569.32 K). Additionally, the influence of the sample purity on the critical temperature was investigated in the same paper. A difference of 2.6 K was observed when decreasing the sample purity from 99.99 % to 99.7 %. Although the hydrocarbons do not behave exactly like hexamethyldisiloxane, these findings show that the purification grade has a large impact on the critical temperature and, therefore, the vapor pressure in the critical region. Thus, the uncertainty of 0.1 MPa (corresponding to 0.5 % − 0.8 %) as specified by the authors [45] has to be questioned. In fact, during the fitting procedure it was not possible to achieve smaller deviations than 2 % from the EOS without compromizing the representation of other properties. Based on these findings, the expected uncertainty of the present EOS regarding the vapor pressure is 0.2 % for $T \leq 410$ K and 2 % for higher temperatures.

Literature shows that the saturated liquid density has been investigated less than the vapor pressure. There are only three different datasets available, which are also very restricted in terms of the temperature range (T = 270 to 360 K). This is insufficient to model the saturated liquid line of hexamethyldisiloxane. Alternatively, the homogeneous density data of Abbas [2] were used. Since no experimental measurements of the saturated vapor line were published, the linear rectilinear diameter ($RD = (\rho' + \rho'')/2$) was applied as a fitting constraint. In Fig. 9, an overview about the available saturated liquid density and homogeneous density data located near the saturated liquid line is given. The data of Abbas [2] were measured close enough to the phase boundary and cover a broader temperature range than the saturated liquid density data. When correlating the present EOS to the dataset of Abbas [2], the saturated liquid density of Gubareva [79] and Mills and MacKenzie [80], which agree well with each other, are reproduced within 0.2 % (AAD = 0.167 % and AAD = 0.109 %, respectively). The data of Guzman *et al.* [58] show a systematic negative offset of about -1.3 %. Unfortunately, no information on the sample purity or the measurement device is available in Ref. [58] so that it is not possible to discuss the reason for this offset.

For all three vapor-liquid equilibrium properties, ancillary equations were developed, which can be used for initial calculations of starting values of iterative phase equilibrium calculations. The equations and the corresponding parameters can be found in the Supplementary Material.

4.4. Assessment of homogeneous state properties

There are several different datasets available for the homogeneous density. Average absolute relative deviations are given in Table 6 and relative deviations from the present EOS are illustrated in Fig. 10. Similar to the vapor pressure, most of the authors reported only a single value to verify their sample purity.

When leaving out these sources, five datasets of Abbas [2], Dickinson [89], Hurd [26], Marcos *et al.* [95], and McLure *et al.* [23] were considered for the development of the present EOS. The data of Dickinson [89] were calculated from a correlation equation based on the available experimental data from literature. Abbas [2] published the only pressure dependent dataset in the liquid phase. All other

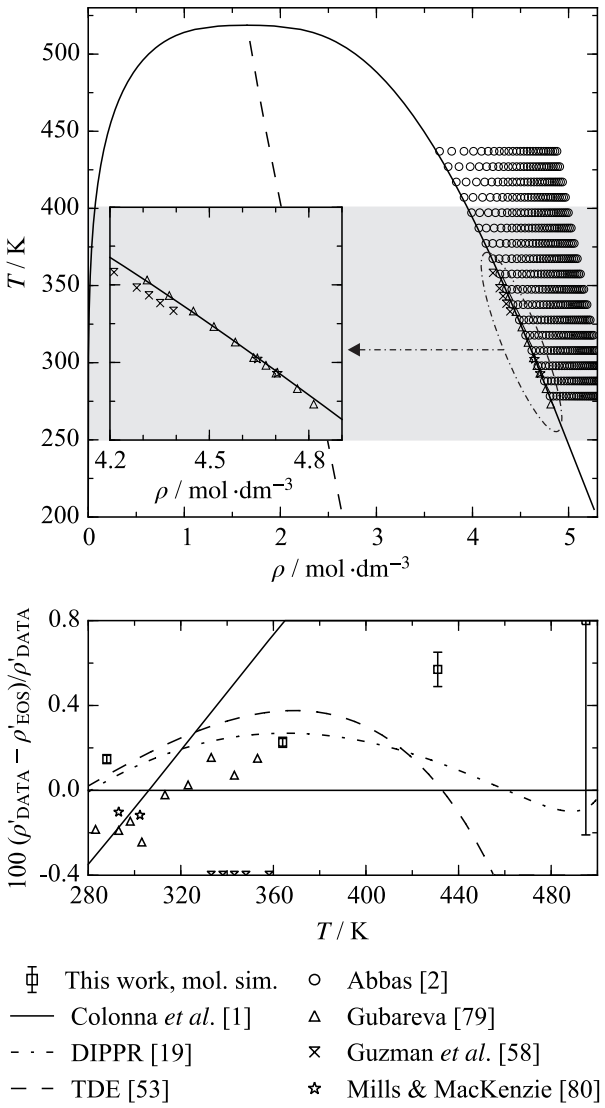

Figure 9: Saturated liquid density of hexamethyldisiloxane. Top: T-ρ diagram including saturated liquid and homogeneous states near the saturated liquid line. Bottom: Relative deviations of experimental saturated liquid density data from the present equation of state.

Table 6: Average absolute relative deviations of the experimental data in the homogeneous region from the present equation of state for hexamethyldisiloxane. All temperatures were adapted to the ITS-90 scale. Datasets, which were applied to the fit, are marked with an asterisk.

	No.	Temperature and		Average absolute relative deviation (AAD) / %						
	of	pressure range				Crit.	Supercritical fluid			
Authors	**data**	T	p	**Gas**	**Liq**	**Reg.**	**LD**	**MD**	**HD**	**overall**
$p\rho T$ **data**										
Abbas [2]*	459	278 - 438	0.9 - 130	-	0.071	-	-	-	-	0.071
Anderson *et al.* [88]	1	293 - 294	0.1 - 1	-	0.120	-	-	-	-	0.120
Bolotov *et al.* [55]	1	293 - 294	0.1 - 1	-	0.081	-	-	-	-	0.081
Dickinson [89][b]	5	303 - 304	100 - 501	-	0.476	-	-	-	-	0.476
Fox *et al.* [90]	1	293 - 294	0.1 - 1	-	0.174	-	-	-	-	0.174
Gaines [91]	1	297 - 298	0.1 - 1	-	1.025	-	-	-	-	1.025
Golik and Cholpan [92]	1	303 - 304	0.1 - 1	-	0.451	-	-	-	-	0.451
Good *et al.* [93]	1	298 - 299	0.1 - 1	-	0.168	-	-	-	-	0.168
Hunter *et al.* [59]	1	298 - 299	0.1 - 1	-	0.122	-	-	-	-	0.122
Hurd [26][b]	3	273 - 314	0.1 - 1	-	0.275	-	-	-	-	0.275
Kaczmarek [63]	1	293 - 294	0.1 - 1	-	0.199	-	-	-	-	0.199
Kaczmarek [94]	1	293 - 294	0.1 - 1	-	0.173	-	-	-	-	0.173
Kaczmarek [64]	1	293 - 294	0.1 - 1	-	0.199	-	-	-	-	0.199
Kaczmarek [65]	1	293 - 294	0.1 - 1	-	0.199	-	-	-	-	0.199
Kaczmarek and Radecki [60]	1	293 - 294	0.1 - 1	-	0.199	-	-	-	-	0.199
Kaczmarek and Radecki [61]	1	293 - 294	0.1 - 1	-	0.199	-	-	-	-	0.199
Killgore *et al.* [66]	1	298 - 299	0.1 - 1	-	0.234	-	-	-	-	0.234
Marcos *et al.* [95]	61	448 - 574	0.1 - 1	0.271	-	-	0.455	-	-	0.365
Matteoli *et al.* [96]	1	298 - 299	0.1 - 1	-	0.089	-	-	-	-	0.089
McLure *et al.* [23]	13	278 - 358	0.1 - 1	-	0.328	-	-	-	-	0.328
Radecki *et al.* [68]	1	293 - 294	0.1 - 1	-	0.383	-	-	-	-	0.383
Radecki and Kaczmarek [69]	1	293 - 294	0.1 - 1	-	0.397	-	-	-	-	0.397
Reuther and Reichel [72]	1	293 - 294	0.1 - 1	-	0.385	-	-	-	-	0.385
Sauer [73]	1	293 - 294	0.1 - 1	-	0.398	-	-	-	-	0.398
Voronkov [76]	1	293 - 294	0.1 - 1	-	0.174	-	-	-	-	0.174
Waterman *et al.* [77]	1	293 - 294	0.1 - 1	-	0.214	-	-	-	-	0.214
Weast and Astle [97]	1	293 - 294	0.1 - 1	-	0.147	-	-	-	-	0.147
Speed of sound w										
This work*	214	365 - 573	0.1 - 30	-	0.174	-	-	-	0.228	0.215
Isobaric heat capacity c_p										
Weast and Astle [97]	1	298 - 299	0.1 - 1	-	0.921	-	-	-	-	0.921
Anderson *et al.* [88]	1	298 - 299	0.1 - 1	-	1.310	-	-	-	-	1.310
Abbas [2]*	32	218 - 374	0.1 - 1	-	0.303	-	-	-	-	0.303
Pedersen *et al.* [67]	8	301 - 346	0.1 - 1	-	0.702	-	-	-	-	0.702
Good *et al.* [93]	1	298 - 299	0.1 - 1	-	0.881	-	-	-	-	0.881
Scott *et al.* [36]*	11	363 - 501	0.0 - 1	0.042	-	-	-	-	-	0.042
Second virial coefficient B^a										
Marcos *et al.* [95]	6	448 - 574	VAP	29.82	-	-	-	-	-	29.82
Scott *et al.* [36]*	3	332 - 374	VAP	35.51	-	-	-	-	-	35.51

[a] AAD of the second virial coefficient B in $\mathrm{cm^3 \cdot mol^{-1}}$

[b] Calculated values

measurements were carried out at atmospheric pressure. Abbas [2] covered a temperature range of 270 to 440 K with a maximum pressure of 130 MPa. A flexural resonator, which was used for the measurements, was calibrated to water (p = 0 MPa to 30 MPa) and heptane (p > 30 MPa). For test purposes, liquid densities of water and heptane were compared to the IAPWS-95 [98] (0.04 %) and the equation of Lemmon and Span [87] (0.08 %). No experimental uncertainty was specified for hexamethyldisiloxane. However, Abbas [2] indicates the uncertainty by referring to the diploma thesis of Schedemann [99], who claimed an uncertainty of 0.7 to 0.8 mg·cm^{-3}.

For hexamethyldisiloxane, these values correspond to a relative deviation of 0.08 % to 0.13 %. When considering this statement as a combined uncertainty, including all relevant irritations during the measurement, the calibration has to be carried out extremely carefully. Keeping in mind the sample purity (99.7 %) and the test measurements on water and heptane, the deviation of 0.2 % from the present equation of state is most probably within the true experimental uncertainty. Therefore, this deviation is also claimed to be the uncertainty of the homogeneous liquid density of the present EOS. Fig. 10, bottom presents the deviations of the homogeneous density data measured at atmospheric pressure. The equation of state of Colonna *et al.* [1] was probably correlated to the data of Hurd [26], because his data point at T = 293.15 K agrees very well with many other data measured at the same temperature. However, these data are not based on real measurements, but were calculated from an equation. For the development of that equation, they measured liquid density data at p = 1 atm. During their measurements they observed a loss of sample, which could be the reason of the different trend in comparison to the dataset of McLure *et al.* [23]. However, in this work none of the data at p = 1 atm were applied to the fit, which leads to a better representation of the data of McLure *et al.* [23] at least in terms of the correct slope and curvature. Their measurements were carried out between T = 278 K and 358 K and a systematic offset of 0.33 % with respect to the present EOS can be observed. In their publication only little information on the experiment is provided and no experimental uncertainty is given. During the fitting procedure, these data were also applied to the fit to reduce the offset. It turned out that it is not possible to improve the representation of these data without increasing deviations to the liquid density data of Abbas [2]. Since the data of Abbas [2] were chosen to be fitted primarily, the data of McLure *et al.* [23] were finally rejected from the fit. Therefore, it is assumed that the systematic offset is caused by the comparatively low purity of the sample (99 %).

The homogeneous gas phase was exclusively investigated by Marcos *et al.* [95]. A bore-tube with a varied volume was used for the measurements. The pressure was obtained with a mercury manometer and the temperature was regulated by two thermopiles. The absence of a measurement device to weigh the sample raises the question how they determined the density of their sample. At least one reference value has to be known, which is commonly measured at atmospheric conditions as explained by Singh and Kudchadker [100].

This value can then be used to calculate the density during the experiment when varying the volume with a constant mass. Fig. 10 shows that these values differ by about 0.5 % in the literature, but no

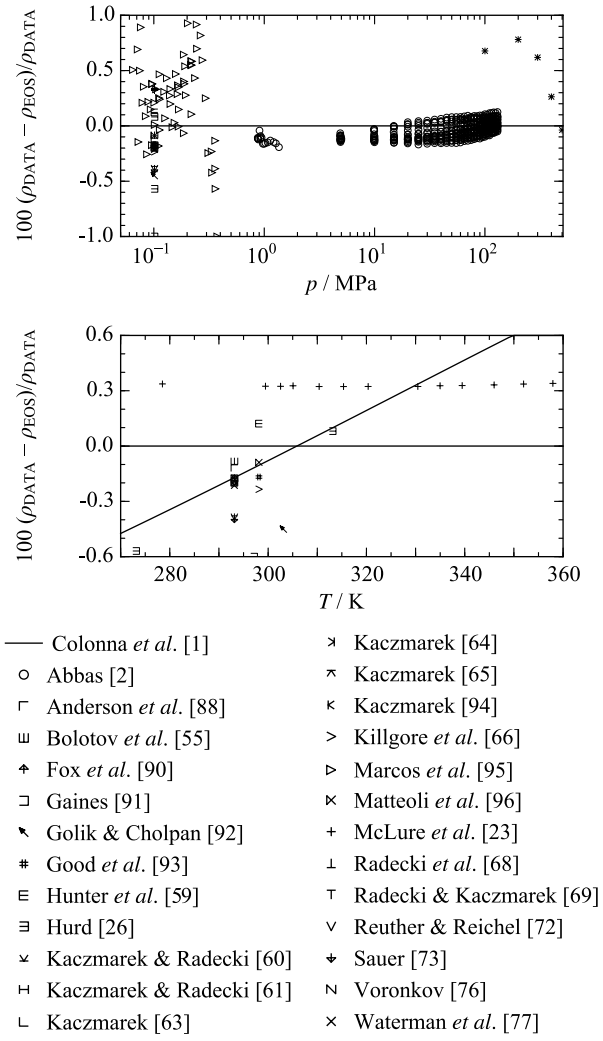

Figure 10: Homogeneous density of hexamethyldisiloxane. Top: Relative deviations of experimental homogeneous density data from the present equation of state. Bottom: Relative deviations of the experimental homogeneous density data at atmospheric pressure from the present equation of state.

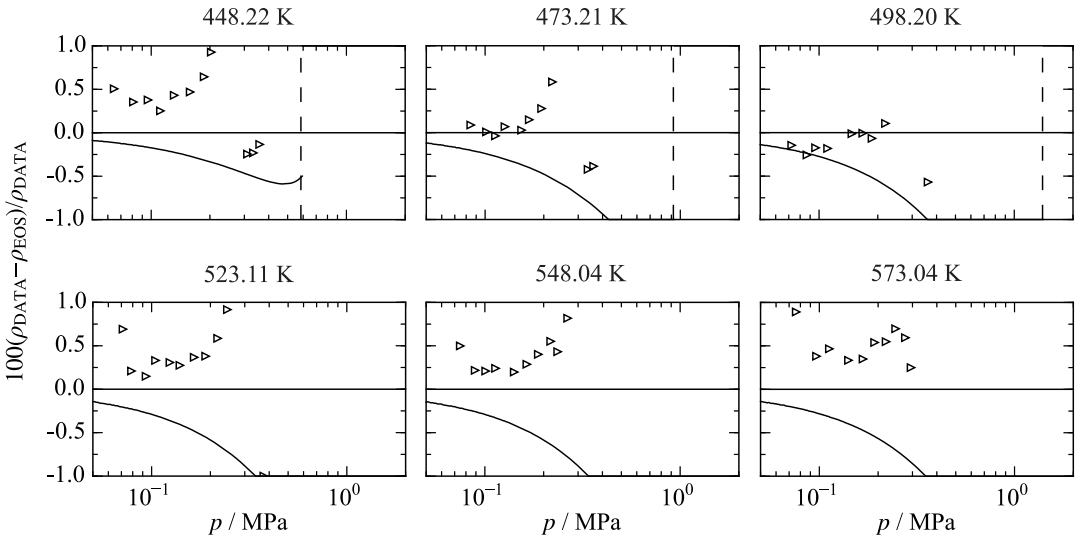

Figure 11: Relative deviations of gaseous $p\rho T$ data of Marcos *et al.* [95] from the present equation of state for hexamethyldisiloxane. — equation of state, Colonna *et al.* [1]; - - phase boundary.

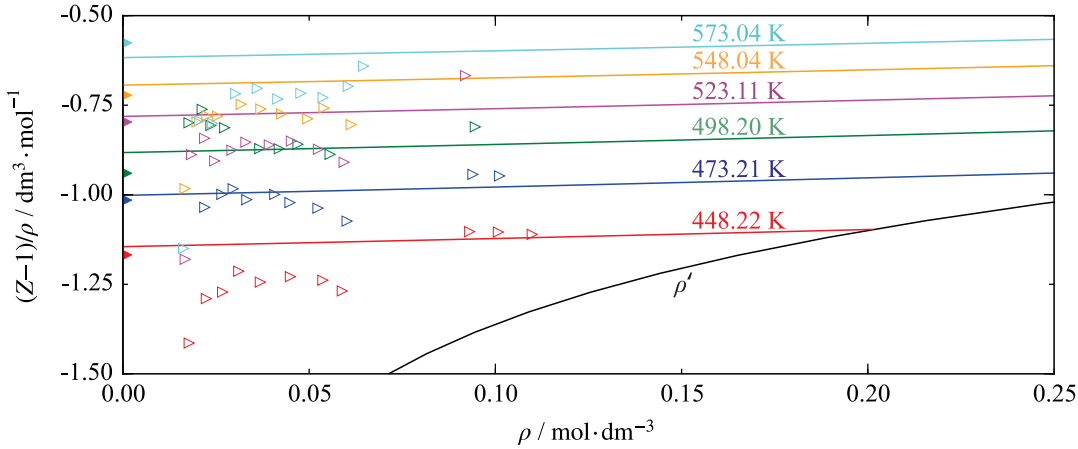

Figure 12: $(Z-1)/\rho - \rho$ diagram of hexamethyldisiloxane: ▷ $p\rho T$ measurements of Marcos *et al.* [95]; ▶ second virial coefficient of Marcos *et al.* [95]; — present equation of state.

value for hexamethyldisiloxane was cited by Marcos *et al.* [95]. Furthermore, they measured a density range of 2 to 18 kg·m^{-3}, which are extremely small values even for state points in the gaseous phase. Therefore, these measurements had to be carried out extremely carefully. Fig. 11 shows that the density data of Marcos *et al.* [95] are reproduced within 1 %, but they are not completely consistent. For a consistency test, the density was recalculated to the compressibility factor $Z = pv/(RT)$ and represented in terms of $(Z-1)/\rho$ as a function of the density in Fig. 12. Six isotherms ranging from 448 K to 573 K are illustrated. For a better assessment, the corresponding isotherms calculated with the present EOS are depicted for orientation. The "high density" data seem to be consistent, at least for the two lowest isotherms. With decreasing density the data start to scatter, which is becoming worse with increasing temperature. The isotherms $T = 448.22$ K and 473.21 K are slightly shifted to lower values with respect to the present EOS. The other isotherms exhibit a larger scatter and even merge. Therefore, the uncertainty specified by Marcos *et al.* [95] (0.33 kPa, corresponding to 0.1 % to 0.5 %) seems to be questionable. Furthermore, a sample purity of 99 % is probably insufficient to carry out these sensitive measurements. Thus, the deviation of 1 % is assumed to be the uncertainty of both the experimental data and present EOS in the gaseous region.

Similar to the approach illustrated in Fig. 12, Marcos *et al.* [95] used their density measurements to extrapolate the second virial coefficient B of each isotherm. They fitted their data to a virial expansion and extrapolated it to $\rho \to 0$ mol·dm^{-3}. The resulting virial coefficient is shown in Fig. 12. When comparing their results for the second virial coefficient with their density measurements, it is not clear how they determined it. Except for the two lowest isotherms the extrapolation does not agree with the underlying dataset. Therefore, these results should be treated carefully. In Fig. 13, absolute deviations of the second virial coefficient data from the present EOS are illustrated. Except for one outlier, the data of Marcos *et al.* [95] and Scott *et al.* [36] are represented within 50 cm^3·mol^{-1}, corresponding to 7 %.

The reason for setting up a new EOS for hexamethyldisiloxane was the finding that the present measurements of the speed of sound deviated by up to 15 % from the equation of Colonna *et al.* [1]. This was caused by the fact the there was no information available on the speed of sound when Colonna *et al.* [1] developed their equation. In this work, new measurements are reported with a combined expanded uncertainty as indicated in Fig. 14. The sample purity of 99 % was not considered for the determination of the experimental uncertainty. These data are reproduced with the present EOS within 0.5 % and most of them are represented within the experimental uncertainty. Therefore, the deviation of 0.5 % is expected to be the uncertainty of the EOS for liquid state speed of sound data.

The only available caloric data in the gaseous region are the heat capacity measurements of Scott *et al.* [36]. They were measured with a low temperature calorimeter as explained by Huffman [101] and no statement on the uncertainty was made. However, these data are reproduced here within 0.1 %, which is most likely well within the expected experimental uncertainty. Further measurements on the isobaric heat capacity are listed in Table 6 and depicted in Fig. 15. There are four different datasets

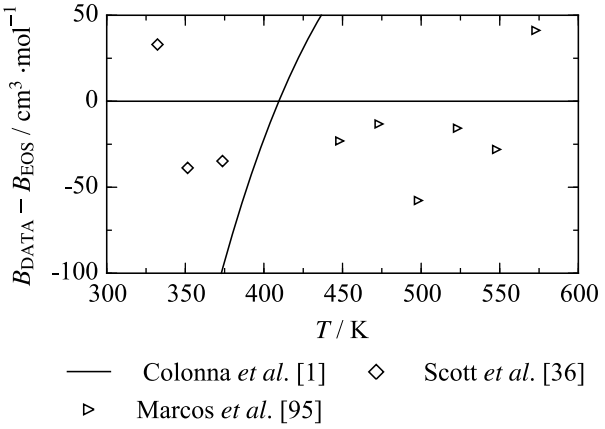

Figure 13: Absolute deviations of the second virial coefficient of Marcos *et al.* [95] and Scott *et al.* [36] from the present equation of state for hexamethyldisiloxane.

available in the liquid region at atmospheric pressure. Anderson *et al.* [88] and Good *et al.* [93] report only single data points and, therefore, they were only considered for comparison. Thus, the results of Abbas [2] and Pedersen *et al.* [67] remained for fitting the present EOS.

A nonsteady hot-wire method was used by Abbas [2], where platinum was employed to heat the sample. The pressure was measured by a diaphragm pressure sensor and the temperature was controlled with a Pt100 thermometer. In this way, results with an experimental uncertainty of 1 % were achieved. The same measurement accuracy was stated by Pedersen *et al.* [67], however, their data are not as consistent as the ones from Abbas [2] and they are restricted to a narrow temperature range. Therefore, the data of Abbas [2] were chosen in the present fitting procedure. These data are represented within 0.5 %, excluding four state points at low temperatures $T < 240$ K. In this way, the data of Pedersen *et al.* [67] are represented within their experimental uncertainty. Finally, Scott *et al.* [36] published saturation heat capacity data c_σ (for the thermodynamic definition see Hoge [102]) measured with the same type of apparatus. They state an experimental uncertainty of 0.2 %, which is probably too low. During the development of the EOS, it turned out that it was not possible to fit these data within the given uncertainty without compromizing the representation of the isobaric heat capacity. Since there are several different datasets available, which agree with each other within the given experimental uncertainty, the homogeneous isobaric heat capacity was chosen to be modeled primarily.

4.5. Assessment of physical and extrapolation behavior

In Fig. 16, typical plots are illustrated to verify the physical and extrapolation behavior of the present EOS. The top, left part of the figure shows the temperature as a function of density along selected isobars ($p_{\min} = 0.5$ MPa, $p_{\max} = 5$ MPa). Additionally, the saturated liquid and vapor curves as well as the rectilinear diameter are presented. It is important that there are no bumps in the course of the isobars, the saturation lines have to meet in a flat maximum, and the rectilinear diameter has to

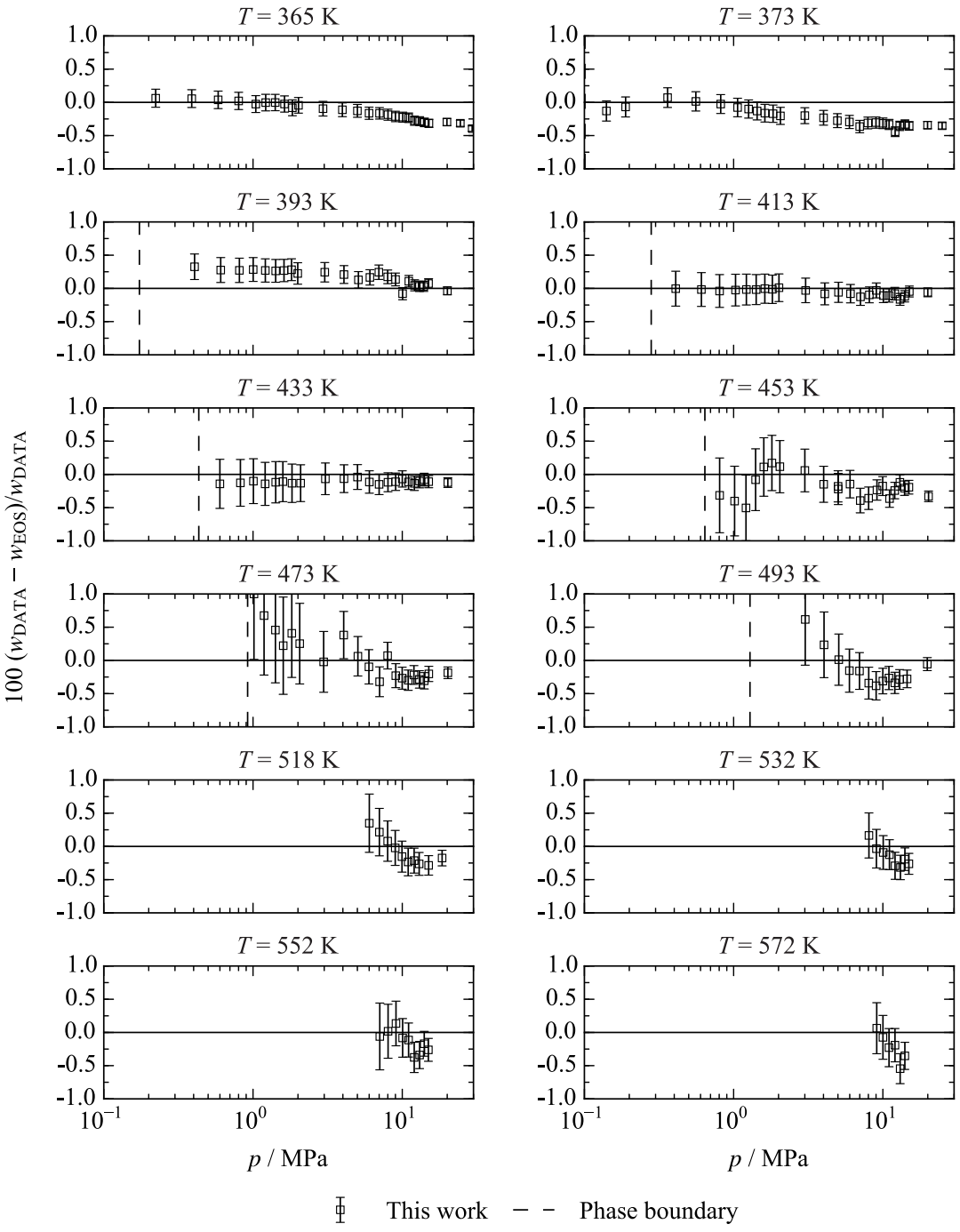

Figure 14: Relative deviations of experimental speed of sound data of this work from the present equation of state for hexamethyldisiloxane.

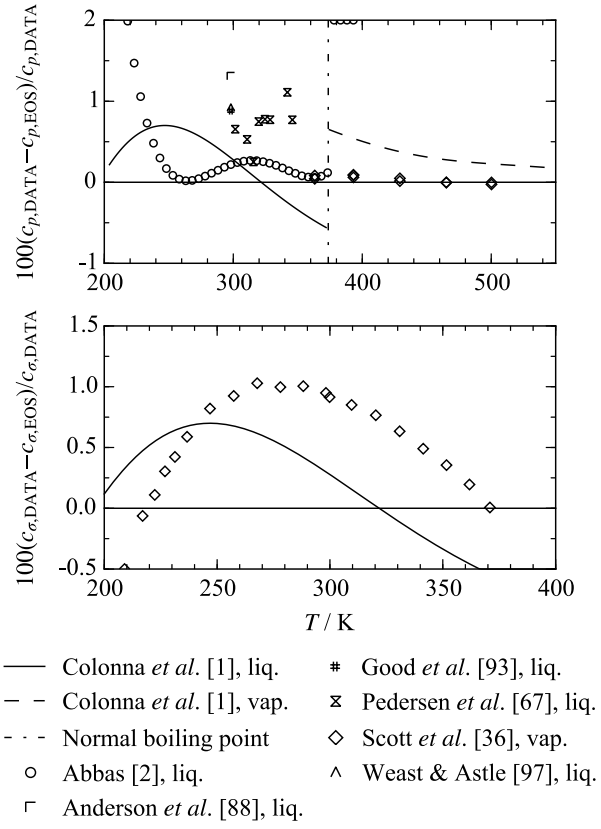

Figure 15: Heat capacities of hexamethyldisiloxane. Top: Relative deviations of experimental isobaric heat capacity data from the present equation of state. — Liquid phase of Colonna *et al.* [1] at $p = 1$ atm; - - vapor phase of Colonna *et al.* [1] at $p = 1$ atm; -.- normal boiling point temperature. Bottom: Relative deviations of experimental saturated heat capacity data from the present equation of state.

be a straight line up to the critical point. The top, right diagram shows the pressure as a function of density along selected isotherms with a maximum temperature of $T = 10^6$ K. Again, bumps have to be avoided and the isotherms have to approach each other at extremely high temperatures, densities and pressures in this double logarithmic plot. In the center of Fig. 16, the residual isochoric heat capacity and the speed of sound is presented. For the isochoric heat capacity, the liquid phase has to exhibit a positive curvature over the whole temperature range for non-associating fluids. When extrapolating it to metastable temperatures below the triple point temperature, the residual isochoric heat capacity has to have a negative slope on the hypothetical liquid side, whereas a positive slope has to be observed in the liquid region approaching the critical temperature. The isochoric heat capacity of the vapor phase has to increase monotonously with increasing temperature. Finally, both phases have to merge with a distinctive peak at the critical point. The speed of sound of the saturated liquid and vapor phase have to have a negative slope and curvature in the vicinity of the critical point. Similar to the maximum of the isochoric heat capacity, the saturation curves of the speed of sound have to merge in a minimum at the critical temperature. Furthermore, the extrapolated liquid phase has to exhibit a negative slope and no curvature, or rather a slightly positive curvature. At the bottom of Fig. 16, the second, third, and fourth thermal virial coefficients are shown as well as some characteristic ideal curves. Detailed information on the behavior of the virial coefficients can be taken from the publication of Thol *et al.* [7]. For the present equation of state, all of the three coefficients show a correct trend. For $T \to 0$ K the virial coefficients have to approach negative infinity. With increasing temperature the virial coefficients have to increase and finally vanish at high temperatures after passing a maximum. The maxima of the third and fourth virial coefficient have to be located in the vicinity of the critical temperature. The characteristic ideal curves (for definition see Span and Wagner [103] or Span [8]) have to be smooth without any bumps. All of the plots presented in Fig. 16 exhibit a reasonable behavior with only small changes in the curvature of the Joule-Thomson inversion curve and the Joule inversion curve. Having in mind the restricted dataset available for hexamethyldisiloxane, the plot of the ideal curves still proves exellent etrapolation behavior.

4.6. Assessment of molecular simulation data

In Fig. 7, the shaded area indicates the region where experimental data are available for hexamethyldisiloxane. On this basis, the range of validity of the present EOS was defined to be $T = 220$ to 570 K with a maximum pressure of $p_{\max} = 130$ MPa. The large scale molecular simulation data presented in this work were applied to the fit to extend the range of validity to a maximum temperature of $T_{\max} = 1200$ K and a maximum pressure of $p_{\max} = 600$ MPa. During these simulations the thermal stability of the fluid was not considered. Therefore, the extended range of validity has to be comprehended as an extrapolation from the real fluid behavior. The temperature of thermal decomposition, which could not be retrieved from literature, was considered irrelevant for the development of the EOS and the fluid was treated as if it is stable throughout.

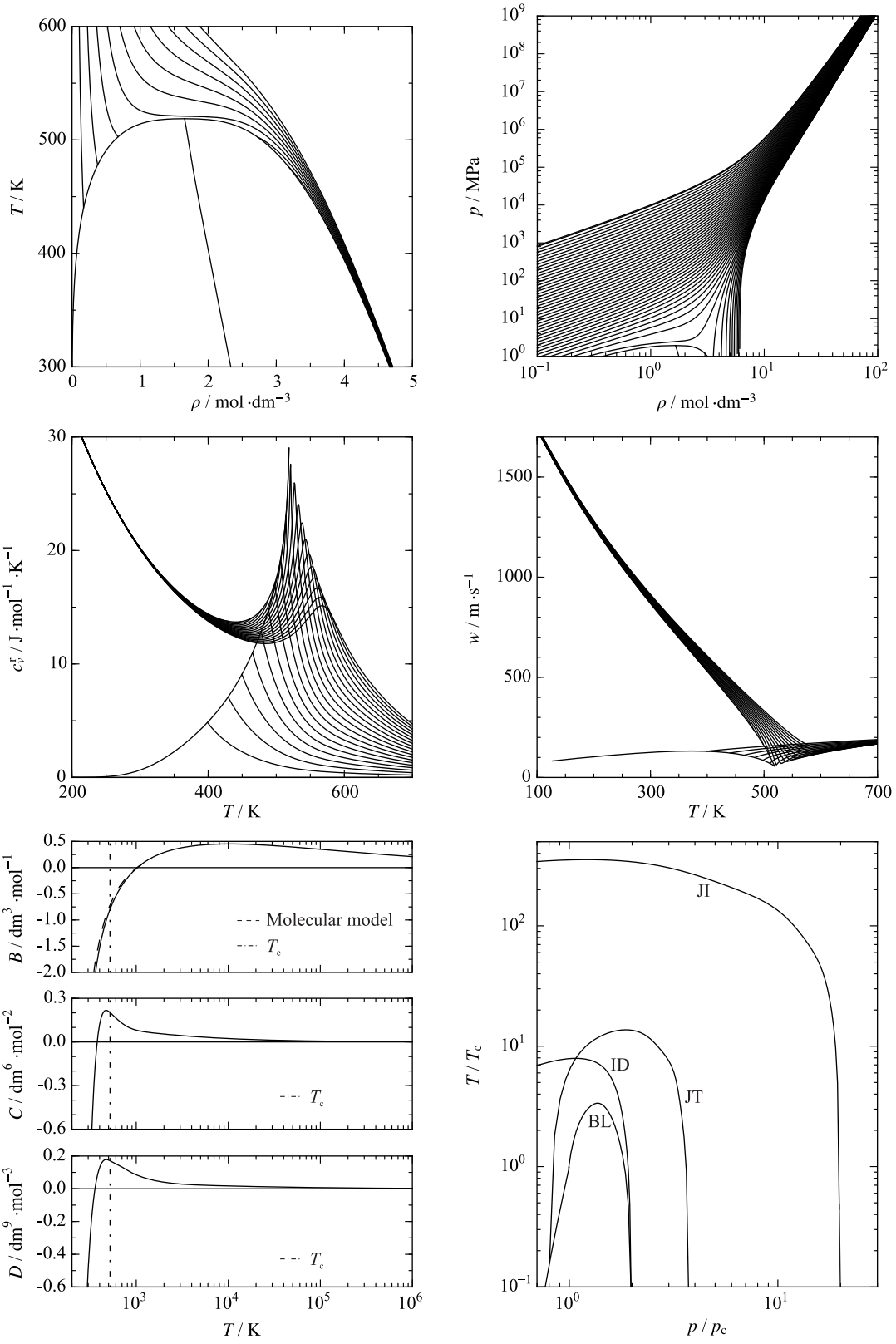

Figure 16: Physical behavior of some thermodynamic properties of hexamethyldisiloxane. Top, left: Isobars and vapor-liquid equilibrium curves together with the rectilinear diameter. Top, right: Pressure as function of density along isotherms at extreme conditions ($T_{\max} = 10^6$ K). Center, left: Residual isochoric heat capacity. Center, right: Speed of sound. Bottom, left: Second, third, and fourth virial coefficients, including B from the molecular interaction model. Bottom, right: Characteristic ideal curves.

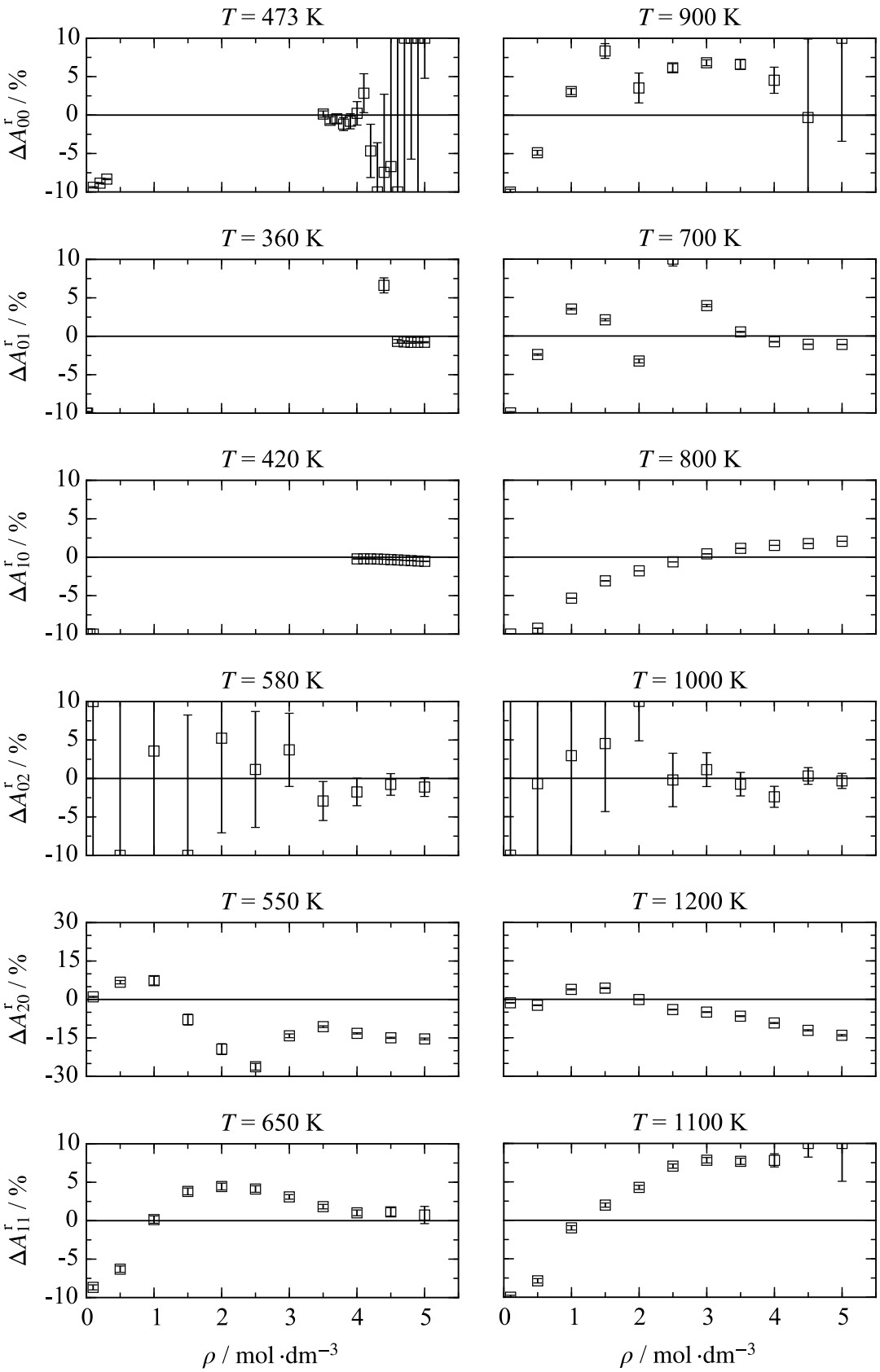

Figure 17: Relative deviations of simulated residual Helmholtz energy derivative data along selected isotherms from the present equation of state for hexamethyldisiloxane. Relative deviations are calculated according to Eq. (12).

In Fig. 17, relative deviations of the simulated residual Helmholtz energy derivatives from the present EOS are shown along selected isotherms. A comprehensive overview including all simulation data is provided in the Supplementary Material. Generally, the uncertainties of the residual Helmholtz energy A^{r}_{00}, the first derivative with respect to the temperature A^{r}_{10}, the first derivative with respect to the density A^{r}_{01}, the first mixed derivative with respect to the temperature and density A^{r}_{11}, and the second derivative with respect to the density A^{r}_{02} are 10 %. The deviations increase with decreasing density and increasing temperature. The second derivative with respect to the temperature A^{r}_{20} was reproduced within 20 %. These values may lead to the assumption that it is not reasonable to apply these data to the fit. However, it has to be kept in mind that these data exclusively represent the residual contribution of the EOS. Common thermodynamic properties, which are usually used for the development of EOS, always include the ideal contribution. Therefore, the ideal contribution of the present EOS was used to recalculate the thermodynamic properties pressure, isochoric heat capacity, isobaric heat capacity, and speed of sound from the residual molecular simulation data according to Eqs. (6) to (8).

In Fig. 18, the resulting data are compared to the present EOS. Additionally, the involved residual Helmholtz energy derivatives are indicated in the grey boxes. Although the deviations of the involved derivatives amount to 10 % or even 20 %, the deviations of the common thermodynamic properties are much smaller. Density data deviate from the present equation of state by no more than 2 %, the isochoric heat capacity is reproduced within 1 %, the isobaric heat capacity is within 2.5 %, and the speed of sound scatters within 4 %. Therefore, residual Helmholtz energy derivatives with uncertainties of up to 20 % are statistically useful values when an extension of validity ranges is aimed at. Keeping in mind that other simulations for validation predicted the available homogeneous liquid density data within their experimental uncertainties, and the speed of sound data within 4 %, the deviations presented in Fig. 18 can be assumed to be a rough estimate of the uncertainty of the present EOS in the extended range of validity. Of course, for a reliable statement further experimental measurements are required in this region.

5. Conclusion

The present EOS is written in terms of the reduced Helmholtz energy and can be used to calculate all thermodynamic equilibrium properties. Reference values are given in the Supplementary Material to verify a computer implementation of the EOS. The underlying set of experimental literature data was extended considerably by the speed of sound measurements that were carried out at 210 state points. In addition, five Helmholtz energy derivatives and the Helmholtz energy itself were predicted by molecular simulation at 194 state points, providing 1164 non-redundant thermodynamic data points for the EOS fit. The range of validity based on the experimental data covers $T = 220$ K to 570 K with a maximum pressure of $p_{\mathrm{max}} = 130$ MPa. By means of molecular simulation data, the temperature and pressure limits were extended to $T_{\mathrm{max}} = 1200$ K and $p_{\mathrm{max}} = 600$ MPa. The expected uncertainty in terms of

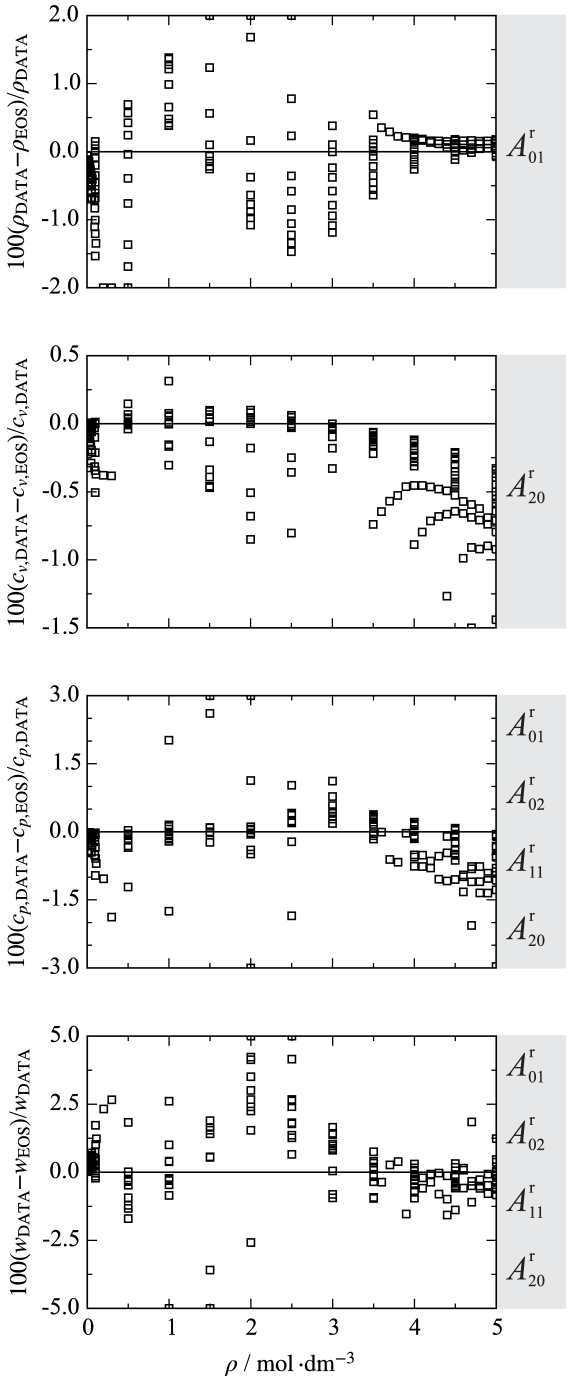

Figure 18: Comparison of several thermodynamic properties obtained from molecular simulation data with the present equation of state for hexamethyldisiloxane. The involved residual Helmholtz energy derivatives are indicated in the grey boxes.

vapor pressure amounts to 0.2 % for $T \leq 410$ K and 2 % for higher temperatures. Homogeneous density data can be calculated with an accuracy of 0.2 % in the liquid phase and 1 % in the gaseous phase. The specified uncertainty for speed of sound data in the liquid phase is 0.5 %. The expected uncertainty of the isobaric heat capacity is 0.2 % in the gaseous phase and 1 % in the liquid phase. The extrapolation behavior was found to be reasonable. For the extended range of validity, only rough estimates on the uncertainty can be made.

6. Acknowlegdements

The authors gratefully acknowledge financial support by Deutsche Forschungsgemeinschaft under the grants VR6/4-1 and SP507/7-1. This work was carried out under the auspices of the Boltzmann-Zuse Society (BZS) of Computational Molecular Engineering. The simulations were performed on the Cray XC40 (Hornet) at the High Performance Computing Center Stuttgart (HLRS) under the grant MMHBF2.

References

[1] P. Colonna, N. R. Nannan, A. Guardone, E. W. Lemmon, Fluid Phase Equilib. 244 (2006) 193–211.

[2] R. Abbas, Anwendung der Gruppenbeitragszustandsgleichung VTPR für die Analyse von reinen Stoffen und Mischungen als Arbeitsmittel in technischen Kreisprozessen, PhD thesis, Technische Universität Berlin, Germany, 2011.

[3] R. Lustig, G. Rutkai, J. Vrabec, Mol. Phys. 113 (2015) 910–931.

[4] G. Rutkai, M. Thol, R. Lustig, R. Span, J. Vrabec, J. Chem. Phys. 139 (2013) 041102.

[5] G. Rutkai, J. Vrabec, Empirical fundamental equation of state for phosgene based on molecular simulation data, J. Chem. Eng. Data.

[6] M. Thol, G. Rutkai, A. Köster, M. Kortmann, R. Span, J. Vrabec, Chem. Eng. Sci. 121 (2015) 87–99.

[7] M. Thol, G. Rutkai, R. Span, J. Vrabec, R. U. Lustig, Int. J. Thermophys. 36 (2015) 25–43.

[8] R. Span, Multiparameter Equations of State: An Accurate Source of Thermodynamic Property Data, Springer Verlag, Berlin, 2000.

[9] P. Kortbeek, M. Muringer, N. Trappeniers, S. Biswas, Rev. Sci. Instrum. 56 (1985) 1269–1273.

[10] F. H. Dubberke, D. B. Rasche, E. Baumhögger, J. Vrabec, Rev. Sci. Instrum. 85 (2014) 084901.

[11] C. Lin, J. Trusler, J. Chem. Phys. 136 (2012) 094511.

[12] S. Ball, J. Trusler, Int. J. Thermophys. 22 (2001) 427–443.

[13] G. Benedetto, R. Gavioso, P. G. Albo, S. Lago, D. M. Ripa, R. Spagnolo, Int. J. Thermophys. 26 (2005) 1667–1680.

[14] F. H. Dubberke, E. Baumhögger, J. Vrabec, Rev. Sci. Instrum. 86 (2015) 054903.

[15] H. Gedanitz, M. Davila, E. Baumhögger, R. Span, J. Chem. Thermodyn. 42 (2010) 478–483.

[16] G. R. Harris, J. Acoust. Soc. Am. 70 (1981) 10–20.

[17] K. Meier, The Pulse-echo Method for High Precision Measurements of the speed of sound in Fluids, Habilitation thesis, Bundeswehruniversität Hamburg, Germany, 2006.

[18] M. W. Schmidt, K. K. Baldridge, J. A. Boatz, S. T. Elbert, M. S. Gordon, J. H. Jensen, S. Koseki, N. Matsunaga, K. A. Nguyen, S. Su, T. L. Windus, M. Dupuis, J. A. Montgomery, J. Comput. Chem. 14 (1993) 1347–1363.

[19] R. Rowley, W. Wilding, J. Oscarson, Y. Yang, N. Zundel, T. Daubert, R. Danner, The DIPPR data compilation of pure compound properties, Design Institute for Physical Properties, AIChE, New York, 2006.

[20] T. Schnabel, A. Srivastava, J. Vrabec, H. Hasse, J. Phys. Chem. B 111 (2007) 9871–9878.

[21] J. Vrabec, J. Stoll, H. Hasse, J. Phys. Chem. B 105 (2001) 12126–12133. doi:10.1021/jp012542o.

[22] J. Stoll, Molecular models for the prediction of thermalphysical properties of pure fluids and mixtures, Fortschritt-Berichte VDI, Reihe 3, vol. 836, VDI-Verlag, Düsseldorf, 2005.

[23] I. A. McLure, A. J. Pretty, P. A. Sadler, J. Chem. Eng. Data 22 (1977) 372–376.

[24] B. Eckl, J. Vrabec, H. Hasse, Mol. Phys. 106 (2008) 1039–1046.

[25] G. Guevara-Carrion, C. Nieto-Draghi, J. Vrabec, H. Hasse, J. Phys. Chem. B 112 (2008) 16664–16674.

[26] C. B. Hurd, J. Am. Chem. Soc. 68 (1946) 364–370.

[27] D. F. Wilcock, J. Am. Chem. Soc. 68 (1946) 691–696.

[28] R. Lustig, Mol. Sim. 37 (2011) 457–465.

[29] R. Lustig, Mol. Phys. 110 (2012) 3041–3052.

[30] S. Deublein, B. Eckl, J. Stoll, S. V. Lishchuk, G. Guevara-Carrion, C. W. Glass, T. Merker, M. Bernreuther, H. Hasse, J. Vrabec, Comp. Phys. Commun. 182 (2011) 2350–2367.

[31] C. W. Glass, S. Reiser, G. Rutkai, S. Deublein, A. Köster, G. Guevara-Carrion, A. Wafai, M. Horsch, M. Bernreuther, T. Windmann, et al., Computer Physics Communications 185 (2014) 3302–3306.

[32] D. Frenkel, B. Smit, Understanding Molecular Simulation: From Algorithms to Applications, Academic Press, Elsevier, San Diego, 2002.

[33] J. A. Barker, R. O. Watts, Mol. Phys. 26 (1973) 789–792.

[34] B. Widom, J. Chem. Phys. 39 (1963) 2808–2812.

[35] A. M. Mosin, A. M. Mikhailov, Zh. Fiz. Khim. 46 (1972) 537.

[36] D. W. Scott, J. F. Messerly, S. S. Todd, G. B. Guthrie, I. A. Hossenlopp, R. T. Moore, A. Osborn, W. T. Berg, J. P. McCullough, J. Phys. Chem. 65 (1961) 1320–1326.

[37] B. K. Harrison, W. H. Seaton, Ind. Eng. Chem. Res. 27 (1988) 1536–1540.

[38] B. E. Poling, J. M. Prausnitz, J. P. O'Connell, The Properties of Gases and Liquids, McGraw-Hill, New York, 2001.

[39] N. R. Nannan, P. Colonna, C. M. Tracy, R. L. Rowley, J. J. Hurly, Fluid Phase Equilib. 257 (2007) 102–113.

[40] L. Haar, J. S. Gallagher, G. S. Kell, Sengers J.V. (ed.), Proc. 8th Symp. Thermophys. Prop., ASME, New York, 1982.

[41] U. Setzmann, W. Wagner, J. Phys. Chem. Ref. Data 20 (1991) 1061–1155.

[42] E. W. Lemmon, R. T. Jacobsen, J. Phys. Chem. Ref. Data 34 (2005) 69–108.

[43] E. W. Lemmon, M. O. McLinden, W. Wagner, J. Chem. Eng. Data 54 (2009) 3141–3180.

[44] E. W. Lemmon, W. Wagner (2015).

[45] I. A. McLure, E. Dickinson, J. Chem. Thermodyn. 8 (1976) 93–95.

[46] P. J. Mohr, B. N. Taylor, D. B. Newell, Rev. Mod. Phys. 84 (2012) 1527–1605.

[47] M. E. Wieser, M. Berglund, Pure Appl. Chem. 81 (2009) 2131–2156.

[48] E. Dickinson, I. A. McLure, B. H. Powell, J. Chem. Soc. Faraday Trans. 1 70 (1974) 2321–2327.

[49] I. A. McLure, J. F. Neville, J. Chem. Thermodyn. 9 (1977) 957–961.

[50] E. D. Nikitin, P. A. Pavlov, A. P. Popov, J. Chem. Thermodyn. 26 (1994) 1047–1050.

[51] C. Young, J. Chem. Thermodyn. 4 (1972) 65–75.

[52] C. Young, J. Chem. Soc., Faraday Trans. 2, 68 (1972) 452–459.

[53] M. Frenkel, R. D. Chirico, V. Diky, K. Kroenlein, C. D. Muzny, A. F. Kazakov, J. W. Magge, I. M. Abdulagatov, E. W. Lemmon, NIST Standard Reference Database 103b: NIST Thermo–Data Engine – Pure Compounds, Binary Mixtures, Reactions, Version 8.0, National Institute of Standards and Technology, Standard Reference Data Program, Gaithersburg, 2013.

[54] R. A. Benkeser, H. R. Krysiak, J. Am. Chem. Soc. 76 (1954) 6353–6357.

[55] B. A. Bolotov, T. V. Orlova, N. P. Kharitonov, N. N. Shenberg, E. A. Batyaev, N. P. Usacheva, J. General Chem. (USSR) 40 (1970) 802–806.

[56] O. L. Flaningam, D. E. Williams, US-Patent, Pat. No. US 5,478,493 (1995) 1–6.

[57] O. L. Flaningam, J. Chem. Eng. Data 31 (1986) 266–272.

[58] J. Guzman, A. S. Teja, W. B. Kay, Fluid Phase Equilib. 7 (1981) 187–195.

[59] M. J. Hunter, E. L. Warrick, J. F. Hyde, C. C. Currie, J. Am. Chem. Soc. 68 (1946) 2284–2290.

[60] B. Kaczmarek, A. Radecki, Pol. J. Chem. 52 (1978) 431–434.

[61] B. Kaczmarek, A. Radecki, Pol. J. Chem. 61 (1987) 267–271.

[62] B. Kaczmarek, A. Radecki, J. Chem. Eng. Data 34 (1989) 195–197.

[63] B. Kaczmarek, Pol. J. Chem. 57 (1983) 617–619.

[64] B. Kaczmarek, J. Chem. Eng. Data 30 (1985) 249–251.

[65] B. Kaczmarek, Pol. J. Chem. 72 (1998) 1120–1123.

[66] C. A. Killgore, W. W. Chew, V. Orr, J. Chem. Eng. Data 11 (1966) 535–537.

[67] M. J. Pedersen, W. B. Kay, H. C. Hershey, J. Chem. Thermodyn. 7 (1975) 1107–1118.

[68] A. Radecki, B. Kaczmarek, J. Grzybowski, J. Chem. Eng. Data 20 (1975) 163–165.

[69] A. Radecki, B. Kaczmarek, J. Chem. Eng. Data 20 (1975) 378–381.

[70] A. Radecki, B. Kaczmarek, J. Chem. Eng. Data 22 (1977) 168–171.

[71] A. Radecki, B. Kaczmarek, J. Chem. Eng. Data 25 (1980) 230–232.

[72] H. Reuther, G. Reichel, Chem. Tech. 6 (1954) 479–480.

[73] R. O. Sauer, J. Am. Chem. Soc. 66 (1944) 1707–1710.

[74] J. L. Speier, J. Am. Chem. Soc. 70 (1948) 4142–4143.

[75] D. R. Stull, Ind. Eng. Chem. 39 (1947) 517–540.

[76] M. G. Voronkov, J. General Chem. (USSR) 29 (1959) 890–896.

[77] H. I. Waterman, W. V. Herwijen, H. W. Denhartog, J. Appl. Chem. 8 (1958) 625–631.

[78] W. Zhang, N. Meng, R. Sun, C. Li, J. Chem. Eng. Data 56 (2011) 5078–5080.

[79] A. Gubareva, Oniitekhim, Code 874 KHP - D83 (1983) 1–6.

[80] A. P. Mills, C. A. MacKenzie, J. Am. Chem. Soc. 76 (1954) 2672–2673.

[81] G. Waddington, J. W. Knowlton, D. W. Scott, G. D. Oliver, S. S. Todd, W. N. Hubbard, C. J. Smith, H. M. Huffman, J. Am. Chem. Soc. 71 (1949) 797–808.

[82] D. R. Stull, Ind. Eng. Chem. Anal. Ed. 18 (1946) 234–242.

[83] E. Dickinson, I. A. McLure, J. Chem. Soc. Faraday Trans. 1 70 (1974) 2313–2320.

[84] Sigma-Aldrich Co. LLC (August 2015). [link].
URL https://www.sigmaaldrich.com

[85] Merck Millipore Corporation (August 2015). [link].
URL http://www.merckmillipore.com

[86] Alfa Aesar GmbH & Co KG (August 2015). [link].
URL http://www.alfa.com

[87] E. W. Lemmon, R. Span, J. Chem. Eng. Data 51 (2006) 785–850.

[88] R. Anderson, B. Arkles, G. L. Larson, Silicon Compounds: Register and Review, Huls America Inc., Piscataway, 1991.

[89] E. Dickinson, J. Phys. Chem. 81 (1977) 2108–2113.

[90] H. W. Fox, P. W. Taylor, W. A. Zisman, Ind. Eng. Chem. 39 (1947) 1401–1409.

[91] G. L. Gaines-Jr., J. Phys. Chem. 73 (1969) 3143–3150.

[92] O. Z. Golik, P. P. Cholpan, Ukr. Fiz. Zh. (Ukr. Ed.) 5 (1960) 242–251.

[93] W. D. Good, J. L. Lacina, B. L. DePrater, J. P. McCullough, J. Phys. Chem. 68 (1964) 579–586.

[94] B. Kaczmarek, Inz. Chem. Procesowa 4 (1983) 497–502.

[95] D. H. Marcos, D. D. Lindley, K. S. Wilson, W. B. Kay, H. C. Hershey, J. Chem. Thermodyn. 15 (1983) 1003–1014.

[96] E. Matteoli, P. Gianni, L. Lepori, A. Spanedda, J. Chem. Eng. Data 56 (2011) 5019–5027.

[97] R. C. Weast, M. J. Astle, CRC Handbook of Data on Organic Compounds, CRC Press, Boca Raton, 1985.

[98] W. Wagner, A. Pruß, J. Phys. Chem. Ref. Data 31 (2002) 387–535.

[99] A. Schedemann, Aufbau und Inbetriebnahme einer Dichtemessanlage. Messung und Modellierung des PVT-Verhaltens bis zu Drücken von 1400 bar, PhD thesis, Universität Oldenburg, Germany, 2009.

[100] R. P. Singh, A. P. Kudchadker, J. Chem. Thermodyn. 11 (1979) 205–213.

[101] H. M. Huffman, Chem. Rev. 40 (1947) 1–14.

[102] H. J. Hoge, J. Res. Natl. Bur. Stand. (U.S.) 36 (1946) 111–118.

[103] R. Span, W. Wagner, Int. J. Thermophys. 18 (1997) 1415–1443.

Supporting Information to: Fundamental equation of state correlation for hexamethyldisiloxane based on experimental and molecular simulation data

M. Thol[1], F. H. Dubberke[2], G. Rutkai[2], T. Windmann[2], A. Köster[2], R. Span[1], and J. Vrabec * [2]

[1]*Lehrstuhl für Thermodynamik, Ruhr-Universität Bochum, 44801 Bochum, Germany*
[2]*Lehrstuhl für Thermodynamik und Energietechnik, Universität Paderborn, 33098 Paderborn, Germany*

Ancillary equations

For computer calculations it is helpful to use ancillary equations to generate starting values for density iterations. Therefore, ancillary equations for vapor pressure, saturated liquid density, and saturated vapor density were developed. The equations and parameters are given below. These ancillary equations are no reference equations so that the fundamental equation of state for hexamethyldisiloxane has to be used to calculate accurate saturation properties.

Vapor pressure:

$$\ln \frac{p_v}{p_c} = \frac{T_c}{T} \sum_{i=1}^{5} n_i \left(1 - \frac{T}{T_c}\right)^{t_i}. \tag{1}$$

Saturated liquid density:

$$\frac{\rho'}{\rho_c} = 1 + \sum_{i=1}^{5} n_i \left(1 - \frac{T}{T_c}\right)^{t_i}. \tag{2}$$

Saturated vapor density:

$$\ln \frac{\rho''}{\rho_c} = \sum_{i=1}^{6} n_i \left(1 - \frac{T}{T_c}\right)^{t_i}. \tag{3}$$

*Corresponding author: Jadran Vrabec, Warburger Str. 100, 33098 Paderborn, Germany, Tel.: +49-5251/60-2421, Fax: +49-5251/60-3522, Email: jadran.vrabec@upb.de

Table 1: Parameter values of the present ancillary equations for vapor pressure, saturated liquid density, and saturated vapor density.

	Eq. (1)		Eq. (2)		Eq. (3)	
i	n_i	t_i	n_i	t_i	n_i	t_i
1	−0.85023E+01	1	0.4003E+01	0.436	−0.37421E+01	0.428
2	0.38030E+01	1.5	−0.6406E+01	0.827	−0.37087E+02	1.79
3	−0.34150E+01	1.98	0.1150E+02	1.24	0.75460E+02	2.28
4	−0.46790E+01	3.86	−0.1004E+02	1.7	−0.71670E+02	2.8
5	−0.31060E+01	14.6	0.4000E+01	2.23	−0.68690E+02	7
6					−0.17840E+03	15.4

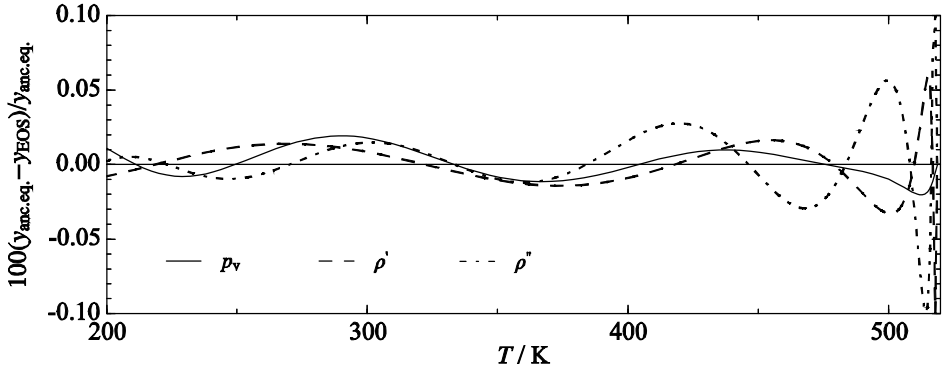

Figure 1: Relative deviations between the ancillary equations and the present fundamental equation of state.

Simulation details

Vapor-liquid equilibrium

The Grand Equilibrium Monte Carlo (MC) method [1] was used for vapor-liquid equilibrium calculations, for which the liquid NpT ensemble runs had 400 000 production steps. The chemical potential was determined by inserting 3 456 virtual molecules into the simulation volume using Widoms test particle method [2]. The pseudo-μVT ensemble vapor simulations, that correspond to the liquid runs, continued with an average of 500 molecules using 200 000 production steps.

Properties in the homogeneous fluid region

The presented $p\rho T$ and speed of sound w data were obtained directly from NpT ensemble MC simulations with 864 molecules using 200 000 production steps, while residual Helmholtz energy derivatives A^{r}_{xy} were determined in NVT ensemble MC simulations with 864 particles using 1 500 000 production steps. The second virial coefficient B was calculated with a dedicated numerical integration scheme [3].

Transport properties

To calculate shear viscosity ν and thermal conductivity λ data, first NpT molecular dynamics simulations were carried out at specified temperature and pressure to obtain the corresponding density (500 000 production time steps). In the second step, NVT MD simulations were carried out at the corresponding temperature and density to calculate the transport properties using 3 500 000 to 7 000 000 time steps for production runs. The simulation length was chosen to obtain at least 20 000 independent time origins of the autocorrelation functions. The sampling length of the autocorrelation functions was chosen to be between 6 und 24 ps, depending on the long-time behavior of the shear viscosity autocorrelation function.

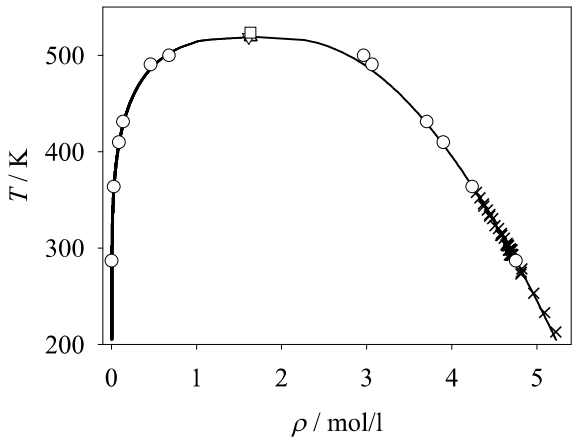

Figure 2: Saturated vapor-liquid densities: (○) simulation data, this work; (×) experimental data [4, 5]; (□) critical point of the present molecular model; (△), (▽) experimental critical point [4, 5] ; (—) correlation of experimental data from the DIPPR database [5].

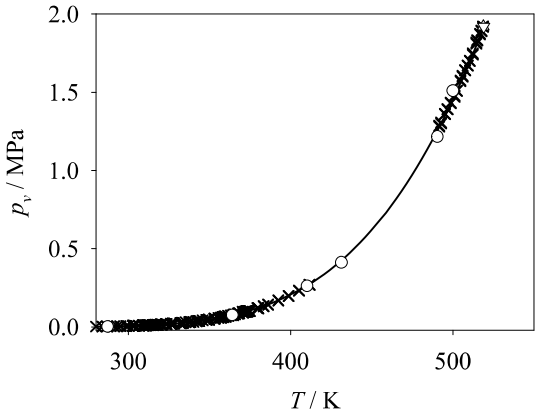

Figure 3: Vapor pressure: (○) simulation data, this work; (×) experimental data [4, 5]; (△), (▽) experimental critical point [4, 5]; (—) correlation of experimental data from the DIPPR database [5].

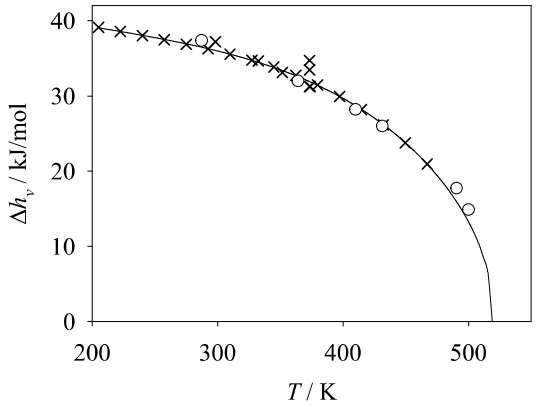

Figure 4: Enthalpy of vaporization: (○) simulation data, this work; (×) experimental data [4, 5]; (—) correlation of experimental data from the DIPPR database [5].

Table 2: Simulation results for vapor-liquid equilibria: p_v vapor pressure; ρ' saturated liquid density; ρ'' saturated vapor density; Δh_v enthalpy of vaporization. Numbers in parentheses denote uncertainties in the last digits.

T [K]	p_v [MPa]	ρ' [mol/l]	ρ'' [mol/l]	Δh_v [kJ/mol]
287.1	0.0033	4.750 (2)	0.0014 (2)	37.38 (1)
364.0	0.076 (2)	4.237 (2)	0.0264 (6)	32.01 (1)
431.3	0.412 (4)	3.703 (3)	0.136 (2)	26.00 (2)
410.0	0.26 (2)	3.898 (5)	0.087 (8)	28.22 (2)
490.5	1.22 (2)	3.06 (2)	0.458 (8)	17.73 (5)
500.0	1.51 (4)	2.96 (20)	0.675 (20)	14.9 (1)

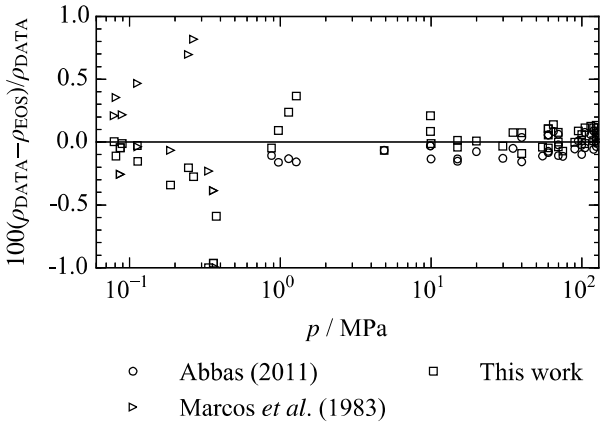

Figure 5: Relative deviations between experimental homogeneous liquid density data of Abbas [6] and Marcos et al. [7] and the present equation of state.

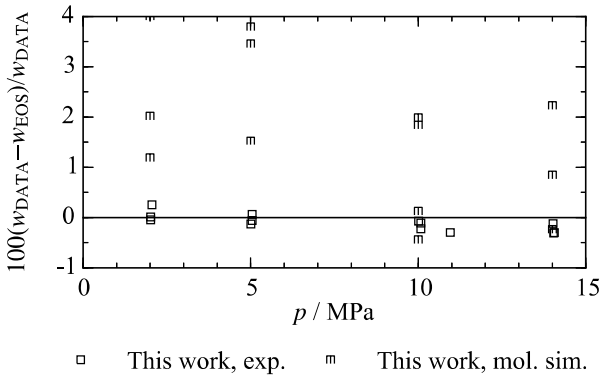

Figure 6: Relative deviations between experimental speed of sound data of this work and the present equation of state.

Table 3: Simulation results for $p\rho T$ data. Numbers in parentheses denote uncertainties in the last digits.

T [K]	p [MPa]	ρ [mol/l]	T [K]	p [MPa]	ρ [mol/l]
278.3	44.944	5.081 (1)	367.41	84.848	4.9041 (8)
278.31	24.981	4.9757 (9)	397.2	44.932	4.5478 (7)
278.32	64.896	5.174 (1)	397.2	64.896	4.6849 (6)
278.32	84.832	5.254 (1)	397.2	104.892	4.8953 (7)
278.32	104.898	5.325 (1)	397.2	129.892	4.9997 (6)
278.33	129.898	5.4003 (9)	397.21	24.975	4.367(1)
307.89	24.947	4.822 (1)	397.21	84.834	4.7967 (6)
307.89	44.918	4.9430 (9)	427.05	24.969	4.215 (2)
307.9	64.882	5.045 (1)	427.05	44.930	4.425 (2)
307.9	84.838	5.1334 (9)	427.05	64.894	4.574 (2)
307.9	104.906	5.210 (1)	427.06	84.830	4.694 (2)
307.9	129.902	5.2961 (9)	427.06	104.890	4.794 (1)
337.63	24.967	4.6689 (9)	427.06	129.906	4.906 (1)
337.63	44.930	4.8087 (7)	437	1.359	3.688 (5)
337.63	104.898	5.1009 (6)	377.31	0.996	4.152 (2)
337.63	129.890	5.1928 (8)	278.3	0.874	4.811 (3)
337.64	64.886	4.9206 (6)	448.26	0.203	0.05800 (2)
337.64	84.832	5.0167 (9)	448.26	0.360	0.1087 (1)
367.4	24.977	4.517 (1)	448.26	0.065	0.01770 (1)
367.4	44.946	4.6769 (8)	498.28	0.219	0.05530 (2)
367.4	104.908	4.9957 (8)	278.5	0.101	4.800 (5)
367.4	129.898	5.0952 (7)	320.36	0.101	4.531 (2)
367.41	64.906	4.8018 (8)	357.96	0.101	4.276 (3)

Table 4: Simulation results for speed of sound w. Numbers in parentheses denote uncertainties in the last digits.

T [K]	p [MPa]	w [10^3 m/s]
365.15	10	0.76 (1)
365.15	14	0.80 (1)
365.15	2	0.68 (3)
365.15	5	0.72 (1)
413.15	10	0.65 (1)
413.15	14	0.69 (1)
413.15	2	0.53 (2)
413.15	5	0.59 (1)
473.15	10	0.50 (1)
473.15	14	0.57 (1)
473.15	2	0.34 (2)
473.15	5	0.42 (1)
573.15	10	0.33 (1)

Table 5: Numerical results for the second virial coefficient B.

T [K]	B [l/mol]	T [K]	B [l/mol]
220	-7.7605	660	-0.3602
230	-6.5832	710	-0.2804
240	-5.6713	760	-0.2147
245	-5.2902	810	-0.1595
250	-4.9493	860	-0.1126
255	-4.643	910	-0.0722
260	-4.3667	960	-0.0372
270	-3.8887	1010	-0.0065
280	-3.4907	1060	0.0207
290	-3.1552	1110	0.0448
300	-2.8691	1160	0.0664
310	-2.6227	1210	0.0858
360	-1.7766	1260	0.1034
410	-1.2861	1310	0.1194
460	-0.9684	1360	0.1339
510	-0.7468	1410	0.1472
560	-0.5837	1460	0.1594
610	-0.4588	1500	0.1685

Table 6: Simulation results for the shear viscosity ν and the thermal conductivity λ. Numbers in parentheses denote uncertainties in the last digits.

T [K]	p [MPa]	ν [mPa $\cdot$ s]	T [K]	p [MPa]	λ [W/(m $\cdot$ s)]
280	0.1	0.45 (3)	295.24	10.0384	0.09 (1)
290	0.1	0.49 (3)	295.38	5.7445	0.12 (1)
295	0.1	0.39 (3)	295.50	0.2394	0.09 (1)
315	0.1	0.34 (2)	362.56	0.571	0.082 (8)
320	0.1	0.31 (2)	362.82	6.1037	0.088 (8)
340	0.1	0.26 (2)	362.84	9.7747	0.090 (9)
350	0.1	0.23 (1)	410.97	5.9604	0.073 (7)
			411.15	9.9404	0.080 (8)
			411.52	0.6564	0.064 (6)
			459.53	1.2543	0.062 (8)
			459.71	5.9081	0.062 (6)
			459.75	9.8705	0.05 (1)
			507.37	2.2843	0.034 (4)
			507.51	5.9243	0.047 (7)
			507.56	10.0179	0.058 (5)

Table 7: Experimental results for the speed of sound w. Δ denotes the uncertainty.

T [K]	p [MPa]	w [m/s]	$\pm\Delta_w$ [m/s]	T [K]	p [MPa]	w [m/s]	$\pm\Delta_w$ [m/s]
365.150	0.223	648.18	0.44	373.276	0.141	618.48	0.47
365.117	0.388	650.58	0.44	373.318	0.189	619.44	0.47
365.130	0.584	653.15	0.43	373.255	0.361	623.09	0.46
365.143	0.801	656.00	0.42	373.335	0.558	625.39	0.46
365.152	1.044	658.99	0.42	373.386	0.819	628.79	0.45
365.162	1.216	661.44	0.41	373.436	1.063	631.82	0.44
365.171	1.409	664.01	0.41	373.453	1.260	634.45	0.44
365.172	1.625	666.75	0.40	373.467	1.437	636.72	0.43
365.168	1.835	669.16	0.40	373.473	1.620	639.06	0.43
365.167	2.016	671.79	0.40	373.483	1.838	642.02	0.42
365.170	2.944	683.34	0.38	373.487	2.059	644.84	0.41
365.175	3.969	695.88	0.36	373.504	2.999	657.46	0.39
365.174	5.004	708.10	0.34	373.517	4.005	670.20	0.37
365.162	5.990	719.24	0.33	373.525	4.957	681.74	0.36
365.136	7.038	730.98	0.32	373.536	5.968	693.71	0.34
365.116	8.021	741.51	0.31	373.537	6.993	705.11	0.33
365.136	8.999	751.54	0.30	373.550	7.935	716.04	0.32
365.157	10.077	762.42	0.29	373.553	8.992	727.59	0.30
365.167	11.037	771.87	0.28	373.556	10.011	738.27	0.29
365.172	12.058	781.42	0.27	373.553	11.005	748.38	0.29
365.176	13.073	790.97	0.26	373.557	12.084	758.33	0.28
365.183	14.057	799.91	0.26	373.562	12.976	767.68	0.27
365.186	15.089	809.13	0.25	373.569	14.056	778.14	0.26
365.227	19.921	850.39	0.22	373.572	15.006	786.79	0.26
365.215	24.490	886.05	0.21	373.615	19.929	829.85	0.23
365.182	29.400	921.05	0.19	373.653	24.956	869.72	0.21
393.283	20.060	787.87	0.24	413.131	20.002	743.78	0.25
393.302	15.000	741.62	0.27	413.153	15.042	694.95	0.28
393.301	13.945	730.77	0.28	413.146	14.021	683.59	0.29
393.310	13.029	721.36	0.29	413.154	13.033	672.44	0.30
393.299	12.087	711.60	0.29	413.150	12.024	661.62	0.31
393.298	11.064	700.96	0.30	413.150	11.008	649.56	0.32
393.310	10.050	688.34	0.31	413.152	10.077	638.31	0.34
393.302	9.015	677.89	0.33	413.148	9.037	625.78	0.35
393.296	7.984	665.88	0.34	413.162	8.116	613.34	0.37
393.305	6.968	653.73	0.36	413.160	7.078	599.11	0.38
393.302	6.067	641.66	0.37	413.159	6.070	585.10	0.41
393.305	5.083	628.29	0.39	413.148	5.043	569.93	0.43
393.300	4.067	614.66	0.41	413.157	4.082	554.69	0.46
393.310	3.024	599.60	0.44	413.150	3.037	537.60	0.50
393.305	1.993	583.63	0.47	413.140	2.013	519.63	0.54
393.295	1.812	581.11	0.48	413.148	1.819	515.87	0.55
393.304	1.613	577.80	0.48	413.155	1.618	512.13	0.56
393.307	1.418	574.58	0.49	413.157	1.416	508.19	0.57
393.307	1.209	571.18	0.50	413.159	1.217	504.32	0.58
393.303	1.002	567.83	0.51	413.163	1.030	500.58	0.60
393.296	0.810	564.54	0.52	413.161	0.805	496.01	0.61
393.299	0.607	561.09	0.53	413.157	0.608	492.11	0.63
393.299	0.406	557.87	0.54	413.156	0.409	488.05	0.64

T [K]	p [MPa]	w [m/s]	$\pm\Delta_w$ [m/s]	T [K]	p [MPa]	w [m/s]	$\pm\Delta_w$ [m/s]
433.143	20.199	704.12	0.26	453.119	20.234	664.75	0.27
433.135	15.032	650.43	0.30	453.102	14.944	607.46	0.31
433.135	14.017	639.08	0.31	453.102	13.971	595.54	0.32
433.121	13.055	627.66	0.32	453.113	13.003	583.83	0.34
433.114	12.050	615.25	0.33	453.119	12.012	570.13	0.35
433.130	11.019	602.33	0.35	453.123	11.087	556.84	0.37
433.133	10.002	589.21	0.36	453.122	9.972	541.98	0.39
433.138	9.028	575.60	0.38	453.130	9.128	529.01	0.40
433.146	8.020	561.08	0.40	453.125	8.027	511.04	0.43
433.145	6.997	545.48	0.42	453.133	7.053	494.57	0.46
433.132	6.018	530.14	0.45	453.121	6.024	477.44	0.49
433.122	5.012	513.57	0.48	453.114	5.011	457.81	0.54
433.138	4.069	496.42	0.52	453.123	5.022	457.81	0.54
433.147	3.053	476.74	0.57	453.119	4.012	437.03	0.59
433.162	2.084	456.03	0.63	453.144	3.001	414.51	0.67
433.163	1.825	450.26	0.65	453.121	2.041	390.01	0.77
433.153	1.585	444.94	0.67	453.120	1.805	383.63	0.80
433.153	1.419	441.03	0.69	453.116	1.593	377.28	0.83
433.145	1.205	435.88	0.71	453.115	1.404	370.92	0.86
433.144	1.006	431.21	0.73	453.116	1.210	363.43	0.90
433.145	0.823	426.55	0.75	453.120	1.015	357.61	0.94
433.145	0.600	420.80	0.78	453.121	0.806	351.04	0.99
473.102	20.213	629.77	0.28	493.191	19.844	593.08	0.29
473.105	15.055	569.87	0.33	493.190	14.528	526.01	0.35
473.106	14.036	556.15	0.34	493.176	12.905	503.64	0.37
473.115	13.029	542.72	0.36	493.182	12.023	489.43	0.39
473.104	11.971	528.22	0.37	493.177	10.979	473.24	0.41
473.102	10.956	512.84	0.39	493.173	9.994	456.47	0.44
473.095	9.987	497.96	0.41	493.169	9.013	438.61	0.47
473.085	9.045	482.71	0.44	493.193	8.040	420.03	0.50
473.080	7.975	465.45	0.47	493.182	6.973	398.49	0.55
473.106	7.047	446.21	0.50	493.173	5.968	375.32	0.61
473.116	5.978	425.52	0.55	493.174	5.064	352.62	0.68
473.109	5.042	405.43	0.60	493.178	4.034	322.94	0.80
473.109	4.051	382.23	0.68	493.179	3.020	287.90	0.99
473.143	2.973	350.26	0.80				
473.113	2.055	320.78	0.97				
473.110	1.818	312.45	1.04				
473.125	1.594	302.93	1.11				
473.105	1.413	296.17	1.18				
473.127	1.186	286.63	1.28				
473.135	1.015	280.51	1.38				

T [K]	p [MPa]	w [m/s]	$\pm\Delta_w$ [m/s]
518.949	18.487	536.79	0.31
518.954	15.022	490.13	0.36
518.935	12.978	459.55	0.40
518.912	12.009	444.04	0.42
518.878	10.954	425.76	0.44
519.029	9.957	407.33	0.47
519.055	8.971	388.07	0.51
519.043	7.981	366.86	0.56
519.049	7.023	344.25	0.61
519.030	6.014	317.31	0.70
532.986	14.939	467.80	0.37
532.969	14.049	454.67	0.38
532.961	13.113	439.27	0.40
532.963	12.069	421.83	0.43
532.958	11.066	404.55	0.46
532.972	10.053	385.12	0.49
532.983	9.052	364.38	0.53
532.973	8.066	342.46	0.58
532.973	5.027	255.07	0.90
532.970	6.022	289.05	0.75
552.866	14.959	440.37	0.38
552.861	14.033	426.19	0.40
552.857	13.067	409.46	0.42
552.862	12.024	390.91	0.45
552.865	11.022	372.95	0.48
552.866	10.056	353.34	0.51
552.858	9.076	332.26	0.56
552.878	8.033	306.12	0.62
552.858	7.069	279.10	0.70
572.520	14.039	400.36	0.41
572.480	13.055	382.80	0.43
572.462	12.056	365.89	0.46
572.439	10.994	344.89	0.49
572.454	10.013	324.42	0.54
572.418	9.097	303.54	0.58

Table 8: Calculated values from the present EOS for computer implementation verification.

T [K]	ρ [mol/l]	p [MPa]	c_p [J/mol/K]	w [m/s]	h [J/mol]	s [J/mol/K]	a [J/mol]
250	5	2.3550378E+0	2.9008362E+2	1.0683855E+3	−3.8660059E+4	−1.2650073E+2	−7.5058829E+3
250	0.0001	2.0772979E−4	2.1658262E+2	1.1531572E+2	1.7151940E+3	3.8943471E+1	−1.0097972E+4
400	0.05	1.5367468E−1	2.9372934E+2	1.3470433E+2	3.8493817E+4	9.9143201E+1	−4.2369572E+3
400	4.5	4.0937214E+1	3.3940134E+2	9.3021218E+2	1.3672106E+4	1.1063887E+1	1.4939229E+2
560	4.5	1.2302530E+2	3.8727688E+2	1.1328991E+3	8.3661459E+4	1.1931485E+2	−1.0493815E+4

Table 9: Helmholtz energy derivatives obtained from molecular simulation.

T / K	ρ/ mol·dm^{-3}	A^{r}_{00}	ΔA^{r}_{00}	A^{r}_{10}	ΔA^{r}_{10}	A^{r}_{01}	ΔA^{r}_{01}	A^{r}_{20}	ΔA^{r}_{20}	A^{r}_{11}	ΔA^{r}_{11}	A^{r}_{02}	ΔA^{r}_{02}
300.00	0.001	−0.0029332	0.0000215	−0.0078886	0.0000192	−0.0028534	0.0000179	−0.0193585	0.0001000	−0.0078590	0.0000855	−0.0005283	0.0002675
300.00	0.002	−0.0057735	0.0000311	−0.0158234	0.0000247	−0.0057307	0.0000252	−0.0392286	0.0001565	−0.0158322	0.0001569	−0.0002254	0.0004373
300.00	4.700	−5.1534864	0.3926543	−13.8152519	0.0002901	−0.6880545	0.0035107	−1.8086307	0.0069111	−17.0055587	0.0678220	45.1094492	0.8303767
300.00	5.000	19.4471135	0.9929154	−14.8827838	0.0008367	2.8862731	0.0094673	−2.1329532	0.0170480	−16.8829538	0.1924254	73.6363506	2.3473525
360.00	0.005	−0.0089408	0.0000292	−0.0224006	0.0000181	−0.0089184	0.0000251	−0.0416300	0.0001190	−0.0225030	0.0001487	−0.0002703	0.0004778
360.00	0.020	−0.0358598	0.0000692	−0.0903933	0.0000411	−0.0357888	0.0000593	−0.1750414	0.0005120	−0.0913410	0.0005655	−0.0004053	0.0016760
360.00	4.400	−3.7738346	0.1169683	−10.3513978	0.0002374	−0.2508876	0.0024626	−1.4581439	0.0050191	−12.8763466	0.0400882	25.6822515	0.5528163
360.00	4.600	−3.1258817	0.3078862	−10.9327587	0.0002194	1.1929161	0.0028523	−1.5958453	0.0048038	−13.3326557	0.0488923	37.5656706	0.6985254
360.00	4.700	−3.4190575	0.4791242	−11.2213089	0.0002605	2.0887458	0.0033607	−1.6917528	0.0056738	−13.5536066	0.0572111	42.4581557	0.6867347
360.00	4.800	−2.3740611	0.7638056	−11.5056216	0.0002875	3.1214561	0.0035322	−1.7826271	0.0063287	−13.4577822	0.0634900	50.0023781	0.7625173
360.00	4.900	−0.5690146	0.9961740	−11.7833319	0.0003530	4.3046571	0.0037538	−1.9058155	0.0069260	−13.4094072	0.0673093	57.7069852	0.7907255
360.00	5.000	−1.3699659	0.9966692	−12.0522547	0.0003705	5.6500394	0.0042672	−2.0308439	0.0090760	−13.2099096	0.0978532	65.4551893	1.1434002
420.00	0.010	−0.0121650	0.0000304	−0.0298208	0.0000158	−0.0122255	0.0000272	−0.0435829	0.0001015	−0.0298665	0.0001527	0.0008226	0.0006239
420.00	0.050	−0.0610223	0.0000766	−0.1502132	0.0000378	−0.0608065	0.0000665	−0.2313437	0.0005158	−0.1515244	0.0007636	0.0020462	0.0027413
420.00	0.100	−0.1219740	0.0001236	−0.3041936	0.0000842	−0.1214307	0.0000964	−0.5117767	0.0014128	−0.3130433	0.0017392	0.0084810	0.0055012
420.00	4.000	−2.8955754	0.0361260	−7.7193424	0.0002426	−0.4049922	0.0017523	−1.1869214	0.0033201	−9.3484512	0.0291653	14.0766179	0.3369376
420.00	4.100	−2.8799659	0.0594229	−7.9547105	0.0001890	−0.0311384	0.0018386	−1.1985366	0.0030824	−9.7305597	0.0309125	16.7471723	0.3832423
420.00	4.200	−2.8927420	0.0687216	−8.1930225	0.0001765	0.4150897	0.0017750	−1.2349044	0.0034166	−10.0979217	0.0334954	19.9404037	0.3834155
420.00	4.300	−2.7447768	0.1187121	−8.4333008	0.0001581	0.9390307	0.0019516	−1.2786692	0.0035373	−10.3223122	0.0335776	23.5461212	0.4258612
420.00	4.400	−2.4323777	0.2078923	−8.6737172	0.0001733	1.5470945	0.0024418	−1.3376241	0.0038049	−10.5390778	0.0403316	27.4574884	0.4758129
420.00	4.500	−2.5748499	0.2103119	−8.9133123	0.0001691	2.2495969	0.0022551	−1.4162357	0.0038562	−10.7284397	0.0410133	31.8853147	0.4950720
420.00	4.600	−2.4244940	0.5741328	−9.1506373	0.0001866	3.0515376	0.0026861	−1.4981172	0.0042183	−10.8288436	0.0433959	36.3655212	0.5457931
420.00	4.700	−2.2031354	0.4882170	−9.3847223	0.0002472	3.9612227	0.0029643	−1.5892285	0.0053199	−10.8257756	0.0515931	42.1173576	0.5650260
420.00	4.800	−1.0327532	0.9582156	−9.6129054	0.0002234	4.9952026	0.0025463	−1.6965884	0.0056149	−10.7839040	0.0565066	48.2586300	0.6760693
420.00	4.900	5.8398146	0.9107996	−9.8338500	0.0003080	6.1663985	0.0033544	−1.8118106	0.0059032	−10.6742599	0.0618886	54.1575357	0.7284453
420.00	5.000	10.0373451	0.9963488	−10.0475259	0.0003251	7.4684804	0.0034725	−1.9281840	0.0073899	−10.3663590	0.0764819	61.8457521	0.8492435
448.26	0.018	−0.0187575	0.0000332	−0.0459549	0.0000186	−0.0186544	0.0000296	−0.0612334	0.0001223	−0.0461467	0.0002063	−0.0000589	0.0009230
448.26	0.022	−0.0229700	0.0000376	−0.0561565	0.0000171	−0.0227933	0.0000337	−0.0755640	0.0001596	−0.0561836	0.0002397	−0.0024698	0.0010339
448.26	0.027	−0.0280463	0.0000460	−0.0689439	0.0000219	−0.0280316	0.0000406	−0.0926684	0.0001793	−0.0688706	0.0002939	0.0006807	0.0012151
448.26	0.031	−0.0323245	0.0000448	−0.0792383	0.0000247	−0.0320702	0.0000386	−0.1070910	0.0002334	−0.0793917	0.0003522	0.0002744	0.0015335
448.26	0.037	−0.0384975	0.0000507	−0.0946537	0.0000270	−0.0383003	0.0000438	−0.1286727	0.0002672	−0.0943777	0.0004153	0.0011784	0.0016448
448.26	0.045	−0.0468556	0.0000555	−0.1151666	0.0000313	−0.0465155	0.0000476	−0.1577596	0.0003293	−0.1150901	0.0005420	0.0001573	0.0024839

T / K	ρ/ mol·dm^{-3}	A^{r}_{00}	ΔA^{r}_{00}	A^{r}_{10}	ΔA^{r}_{10}	A^{r}_{01}	ΔA^{r}_{01}	A^{r}_{20}	ΔA^{r}_{20}	A^{r}_{11}	ΔA^{r}_{11}	A^{r}_{02}	ΔA^{r}_{02}
448.26	0.054	−0.0560307	0.0000664	−0.1382680	0.0000350	−0.0558584	0.0000548	−0.1907706	0.0003828	−0.1394679	0.0005995	0.0008781	0.0027367
448.26	0.059	−0.0613670	0.0000637	−0.1512765	0.0000408	−0.0609094	0.0000551	−0.2104316	0.0004510	−0.1521506	0.0006872	−0.0012787	0.0027252
448.26	0.093	−0.0964898	0.0000902	−0.2392942	0.0000464	−0.0957389	0.0000760	−0.3465383	0.0008104	−0.2411171	0.0010319	−0.0055438	0.0041967
448.26	0.101	−0.1046743	0.0001033	−0.2600462	0.0000594	−0.1039592	0.0000901	−0.3785411	0.0009206	−0.2649746	0.0013701	0.0014977	0.0044405
448.26	0.110	−0.1140914	0.0000992	−0.2835341	0.0000526	−0.1129799	0.0000830	−0.4166577	0.0011904	−0.2851521	0.0014358	0.0036381	0.0053220
473.00	0.100	−0.0906332	0.0000808	−0.2265358	0.0000365	−0.0898474	0.0000710	−0.2963831	0.0006384	−0.2287649	0.0009389	−0.0065360	0.0044302
473.00	0.200	−0.1798995	0.0001441	−0.4555603	0.0000894	−0.1771710	0.0001132	−0.6545930	0.0019379	−0.4621285	0.0027805	0.0167871	0.0091347
473.00	0.300	−0.2675992	0.0002073	−0.6881818	0.0002661	−0.2615223	0.0001575	−1.1180273	0.0075428	−0.7077711	0.0049616	0.0211102	0.0159596
473.00	3.500	−2.0300848	0.0081779	−5.7436799	0.0003498	−0.6569832	0.0014121	−1.0880156	0.0059058	−6.5005840	0.0242439	5.9947534	0.2298990
473.00	3.600	−2.0288963	0.0091730	−5.9326311	0.0002972	−0.4820524	0.0014294	−1.0502884	0.0042508	−6.8830295	0.0219642	7.2071205	0.2633632
473.00	3.700	−2.0425050	0.0114820	−6.1259869	0.0002262	−0.2736339	0.0014143	−1.0330248	0.0035503	−7.2079874	0.0243589	8.8902877	0.2597617
473.00	3.800	−2.0319052	0.0171751	−6.3231089	0.0001961	−0.0187613	0.0014581	−1.0268846	0.0030009	−7.5729029	0.0231250	10.6937475	0.2744787
473.00	3.900	−2.0354436	0.0199582	−6.5244720	0.0001574	0.2808857	0.0014389	−1.0510374	0.0031468	−7.9239401	0.0234951	12.1042228	0.3167086
473.00	4.000	−2.0441793	0.0311914	−6.7284333	0.0001599	0.6371427	0.0014726	−1.0724543	0.0028176	−8.2050691	0.0240590	14.7698737	0.3007053
473.00	4.100	−2.0771930	0.0525790	−6.9348397	0.0001537	1.0476465	0.0015203	−1.1075668	0.0028553	−8.4852273	0.0245942	17.2050202	0.3263049
473.00	4.200	−1.8977646	0.0658122	−7.1416762	0.0001507	1.5305838	0.0017015	−1.1538019	0.0029606	−8.7054740	0.0271691	20.1848281	0.3671789
473.00	4.300	−1.7526696	0.1122403	−7.3489449	0.0001577	2.0811284	0.0017584	−1.2108203	0.0034267	−8.9119693	0.0327091	23.1300823	0.3975311
473.00	4.400	−1.7561578	0.1784160	−7.5550709	0.0001578	2.7128039	0.0020393	−1.2812852	0.0032929	−9.0844286	0.0323900	26.5468471	0.4004540
473.00	4.500	−1.7028279	0.3565634	−7.7597725	0.0001704	3.4258646	0.0022657	−1.3551829	0.0038195	−9.1811069	0.0393124	30.1808885	0.4870965
473.00	4.600	−0.7519662	0.3222620	−7.9611764	0.0001849	4.2340947	0.0022555	−1.4344492	0.0039556	−9.1123969	0.0426050	36.1647614	0.4994220
473.00	4.700	0.3119353	0.3896846	−8.1581037	0.0002037	5.1438368	0.0022180	−1.5321365	0.0044890	−9.1340151	0.0476506	40.4729225	0.5714158
473.00	4.800	−3.3778780	0.5313412	−8.3490047	0.0002405	6.1728351	0.0027270	−1.6361340	0.0051843	−9.0308643	0.0508285	45.9802162	0.5785250
473.00	4.900	3.2449459	0.6996224	−8.5331302	0.0002656	7.3150721	0.0027912	−1.7353832	0.0060036	−8.7456833	0.0615919	52.8603007	0.6853160
473.00	5.000	18.5670237	0.9682709	−8.7091097	0.0003069	8.5938698	0.0032848	−1.8605036	0.0074597	−8.5129977	0.0742865	58.9930788	0.8041979
498.28	0.018	−0.0144391	0.0000286	−0.0362855	0.0000115	−0.0143284	0.0000256	−0.0412690	0.0000770	−0.0361179	0.0001409	0.0008527	0.0007266
498.28	0.021	−0.0167938	0.0000332	−0.0423230	0.0000127	−0.0167467	0.0000300	−0.0482847	0.0000873	−0.0426496	0.0001656	−0.0018284	0.0009254
498.28	0.024	−0.0192271	0.0000347	−0.0483451	0.0000128	−0.0191106	0.0000313	−0.0552533	0.0000929	−0.0481684	0.0001909	0.0005223	0.0010201
498.28	0.027	−0.0215636	0.0000361	−0.0544129	0.0000148	−0.0215303	0.0000325	−0.0622591	0.0001133	−0.0546500	0.0002226	−0.0010276	0.0009455
498.28	0.037	−0.0295418	0.0000453	−0.0746076	0.0000186	−0.0294344	0.0000402	−0.0857633	0.0001755	−0.0742771	0.0003022	−0.0003833	0.0014623
498.28	0.042	−0.0335897	0.0000480	−0.0846467	0.0000191	−0.0333577	0.0000426	−0.0974424	0.0001809	−0.0849107	0.0003456	−0.0002688	0.0016268
498.28	0.047	−0.0375790	0.0000490	−0.0947143	0.0000224	−0.0372686	0.0000425	−0.1091169	0.0002121	−0.0944156	0.0003749	0.0009357	0.0015937
498.28	0.056	−0.0447399	0.0000529	−0.1128801	0.0000259	−0.0443504	0.0000453	−0.1308955	0.0002521	−0.1125692	0.0004363	0.0039460	0.0019486
498.28	0.095	−0.0755154	0.0000686	−0.1914237	0.0000363	−0.0747946	0.0000562	−0.2270508	0.0005001	−0.1921470	0.0008124	0.0015871	0.0035828
523.15	0.017	−0.0120122	0.0000239	−0.0309332	0.0000101	−0.0119888	0.0000211	−0.0328587	0.0000564	−0.0311003	0.0001124	0.0009881	0.0006501

T / K	ρ/ mol·dm^{-3}	A^{r}_{00}	ΔA^{r}_{00}	A^{r}_{10}	ΔA^{r}_{10}	A^{r}_{01}	ΔA^{r}_{01}	A^{r}_{20}	ΔA^{r}_{20}	A^{r}_{11}	ΔA^{r}_{11}	A^{r}_{02}	ΔA^{r}_{02}
523.15	0.018	−0.0127611	0.0000289	−0.0327600	0.0000108	−0.0126369	0.0000260	−0.0347776	0.0000583	−0.0325264	0.0001294	0.0005134	0.0006595
523.15	0.022	−0.0155781	0.0000285	−0.0400132	0.0000128	−0.0154466	0.0000252	−0.0425633	0.0000724	−0.0402582	0.0001412	−0.0005867	0.0007960
523.15	0.025	−0.0176762	0.0000335	−0.0454674	0.0000140	−0.0176021	0.0000300	−0.0483340	0.0000875	−0.0457405	0.0001628	−0.0022064	0.0008780
523.15	0.029	−0.0205063	0.0000346	−0.0527177	0.0000128	−0.0203601	0.0000309	−0.0560731	0.0000908	−0.0525671	0.0002026	−0.0002260	0.0010032
523.15	0.033	−0.0232872	0.0000391	−0.0600065	0.0000165	−0.0231825	0.0000354	−0.0641051	0.0001196	−0.0599629	0.0002252	0.0013392	0.0011289
523.15	0.039	−0.0275115	0.0000416	−0.0708887	0.0000158	−0.0273818	0.0000368	−0.0755459	0.0001253	−0.0707407	0.0002279	0.0014696	0.0014046
523.15	0.045	−0.0317306	0.0000451	−0.0818228	0.0000197	−0.0315340	0.0000412	−0.0876271	0.0001509	−0.0812792	0.0003401	0.0019227	0.0014417
523.15	0.053	−0.0373837	0.0000520	−0.0963457	0.0000191	−0.0370941	0.0000477	−0.1036498	0.0001874	−0.0964792	0.0003500	−0.0040929	0.0017127
523.15	0.059	−0.0415939	0.0000516	−0.1072966	0.0000204	−0.0411653	0.0000448	−0.1154561	0.0002018	−0.1065115	0.0003928	0.0007923	0.0018857
523.15	0.092	−0.0645624	0.0000636	−0.1670792	0.0000258	−0.0639422	0.0000580	−0.1822388	0.0003057	−0.1659789	0.0006450	−0.0021427	0.0029393
550.00	0.100	−0.0615041	0.0000604	−0.1638690	0.0000253	−0.0608008	0.0000515	−0.1659382	0.0003218	−0.1637238	0.0006259	−0.0052035	0.0029482
550.00	0.500	−0.2942037	0.0002061	−0.8020180	0.0002973	−0.2760959	0.0001642	−0.8984045	0.0058923	−0.7682847	0.0043328	0.0557725	0.0166797
550.00	1.000	−0.5518053	0.0004301	−1.5408533	0.0011736	−0.4782275	0.0003016	−1.8066347	0.0308791	−1.4233938	0.0105476	0.2044643	0.0384929
550.00	1.500	−0.7739635	0.0007401	−2.1876757	0.0015940	−0.6056814	0.0004145	−2.1215993	0.0443956	−1.8072894	0.0172315	0.2783868	0.0526333
550.00	2.000	−0.9571221	0.0011721	−2.7693041	0.0014092	−0.6712437	0.0007292	−1.8580068	0.0394597	−2.3160617	0.0238080	0.6521159	0.0759067
550.00	2.500	−1.1046226	0.0016133	−3.3642783	0.0006586	−0.6479629	0.0008149	−1.2787492	0.0167615	−3.1719398	0.0227928	1.2128568	0.0966951
550.00	3.000	−1.2036545	0.0022871	−4.0382224	0.0003761	−0.4136475	0.0010517	−0.9625047	0.0071299	−4.3062643	0.0206149	2.7105535	0.1318140
550.00	3.500	−1.2232537	0.0063875	−4.8057435	0.0001672	0.2623691	0.0010880	−0.8560010	0.0029082	−5.6595579	0.0166783	6.9524304	0.2085738
550.00	4.000	−1.1068547	0.0322461	−5.6439862	0.0001255	1.7695854	0.0012873	−0.9743700	0.0022387	−6.8135872	0.0220700	15.4087448	0.2902774
550.00	4.500	−0.4200971	0.1740779	−6.4888338	0.0001548	4.6668123	0.0017604	−1.2841613	0.0029648	−7.3064258	0.0313441	30.2850479	0.3783383
550.00	5.000	14.6470194	0.6132261	−7.2356005	0.0002747	9.7198869	0.0030437	−1.7667108	0.0063235	−6.4278196	0.0613531	55.7430704	0.6474740
573.04	0.024	−0.0131154	0.0000453	−0.0363709	0.0000165	−0.0132814	0.0000301	−0.0341453	0.0000496	−0.0361361	0.0000987	0.0010426	0.0006440
573.04	0.030	−0.0166664	0.0000486	−0.0453559	0.0000146	−0.0165014	0.0000386	−0.0426404	0.0000524	−0.0458429	0.0001240	−0.0013911	0.0007975
573.04	0.036	−0.0199468	0.0000557	−0.0543802	0.0000138	−0.0199594	0.0000472	−0.0509044	0.0000647	−0.0547268	0.0001546	0.0036800	0.0009475
573.04	0.042	−0.0231653	0.0000564	−0.0635190	0.0000172	−0.0230938	0.0000431	−0.0595764	0.0000743	−0.0629644	0.0001384	0.0069487	0.0012828
573.04	0.048	−0.0267947	0.0000561	−0.0725469	0.0000181	−0.0263365	0.0000417	−0.0683395	0.0000929	−0.0732032	0.0001924	−0.0011111	0.0012281
573.04	0.054	−0.0301703	0.0000581	−0.0815130	0.0000193	−0.0294496	0.0000448	−0.0765565	0.0001043	−0.0808122	0.0002233	−0.0000099	0.0011706
573.04	0.060	−0.0332549	0.0000736	−0.0905886	0.0000199	−0.0328570	0.0000555	−0.0854169	0.0001154	−0.0904894	0.0002078	−0.0037922	0.0015419
573.04	0.065	−0.0356160	0.0000815	−0.0981075	0.0000241	−0.0355952	0.0000551	−0.0926759	0.0001116	−0.0980444	0.0002201	−0.0012273	0.0011273
580.00	0.100	−0.0533292	0.0000569	−0.1475806	0.0000239	−0.0524789	0.0000509	−0.1373475	0.0002335	−0.1465942	0.0005362	−0.0011047	0.0025787
580.00	0.500	−0.2537342	0.0001742	−0.7196508	0.0001886	−0.2372529	0.0001464	−0.6909872	0.0036690	−0.6907580	0.0032679	0.0210582	0.0129190
580.00	1.000	−0.4746676	0.0003231	−1.3823641	0.0007116	−0.4076188	0.0002458	−1.2923055	0.0161216	−1.2594934	0.0079947	0.1627900	0.0323628
580.00	1.500	−0.6618580	0.0005982	−1.9777397	0.0009357	−0.5132210	0.0004034	−1.5034915	0.0219848	−1.7289802	0.0122317	0.2655751	0.0484708
580.00	2.000	−0.8157832	0.0009418	−2.5442988	0.0009230	−0.5498676	0.0005880	−1.3355904	0.0261598	−2.2796374	0.0177127	0.5667362	0.0697357

T / K	ρ/ mol·dm^{-3}	A_{00}^{r}	ΔA_{00}^{r}	A_{10}^{r}	ΔA_{10}^{r}	A_{01}^{r}	ΔA_{01}^{r}	A_{20}^{r}	ΔA_{20}^{r}	A_{11}^{r}	ΔA_{11}^{r}	A_{02}^{r}	ΔA_{02}^{r}
580.00	2.500	−0.9318399	0.0012463	−3.1311256	0.0005217	−0.4819241	0.0007646	−1.0689800	0.0092150	−3.0445583	0.0160734	1.2123890	0.0914171
580.00	3.000	−1.0010622	0.0022148	−3.7829681	0.0002784	−0.1893912	0.0008675	−0.8370073	0.0039382	−4.1531209	0.0154865	3.1120083	0.1481128
580.00	3.500	−0.9668956	0.0058397	−4.5141644	0.0001224	0.5547021	0.0009614	−0.8105610	0.0021256	−5.3801622	0.0152967	6.9079803	0.1751739
580.00	4.000	−0.8089717	0.0269299	−5.3021108	0.0001142	2.1204579	0.0013484	−0.9523842	0.0020724	−6.4049001	0.0204046	14.9558430	0.2680584
580.00	4.500	−0.5249882	0.2726033	−6.0869323	0.0001504	5.0435374	0.0020410	−1.2586251	0.0031919	−6.7356014	0.0340842	29.4933967	0.4149446
580.00	5.000	9.3591576	0.8732024	−6.7699188	0.0002955	10.0512037	0.0029631	−1.7470741	0.0058274	−5.8807168	0.0599160	53.5465213	0.6555252
600.00	0.100	−0.0483715	0.0000534	−0.1382875	0.0000213	−0.0476853	0.0000474	−0.1225372	0.0001967	−0.1380187	0.0004552	0.0014927	0.0025749
600.00	0.500	−0.2303580	0.0001837	−0.6738912	0.0001702	−0.2142709	0.0001635	−0.6005240	0.0027904	−0.6506620	0.0029521	0.0132508	0.0151407
600.00	1.000	−0.4295128	0.0002954	−1.2965886	0.0005455	−0.3661421	0.0002090	−1.0822274	0.0105546	−1.1844386	0.0059517	0.0958472	0.0292922
600.00	1.500	−0.5967580	0.0004972	−1.8684868	0.0008064	−0.4546493	0.0003584	−1.2631547	0.0153551	−1.6512254	0.0106689	0.2618812	0.0414111
600.00	2.000	−0.7322152	0.0008663	−2.4178068	0.0006776	−0.4741178	0.0006070	−1.1380252	0.0129694	−2.2124973	0.0132408	0.5131351	0.0637527
600.00	2.500	−0.8278546	0.0012110	−2.9932598	0.0004014	−0.3785842	0.0006837	−0.9311662	0.0067700	−3.0095538	0.0122279	1.3995983	0.0927690
600.00	3.000	−0.8718808	0.0019812	−3.6293520	0.0002319	−0.0513716	0.0008101	−0.7856990	0.0039541	−4.0330220	0.0137175	3.1569697	0.1225511
600.00	3.500	−0.8178945	0.0047907	−4.3372028	0.0001504	0.7348294	0.0010589	−0.7846285	0.0020963	−5.1708796	0.0151190	7.3705632	0.1682658
600.00	4.000	−0.6457773	0.0258255	−5.0938894	0.0000986	2.3335021	0.0012998	−0.9356845	0.0021854	−6.1147255	0.0211403	14.9806578	0.2659175
600.00	4.500	−0.1824842	0.2251909	−5.8420115	0.0001267	5.2683307	0.0017441	−1.2470920	0.0029908	−6.3821470	0.0324183	29.5468790	0.4111497
600.00	5.000	3.2556009	0.7013522	−6.4862906	0.0002514	10.2465566	0.0027551	−1.7255146	0.0061057	−5.4710965	0.0609024	53.0108223	0.6492203
650.00	0.100	−0.0381157	0.0000479	−0.1194085	0.0000158	−0.0374020	0.0000427	−0.0944829	0.0001768	−0.1193939	0.0003960	−0.0009350	0.0022567
650.00	0.500	−0.1801197	0.0001664	−0.5821942	0.0001069	−0.1658597	0.0001509	−0.4477515	0.0016135	−0.5600234	0.0022834	0.0297805	0.0125534
650.00	1.000	−0.3322991	0.0002811	−1.1271188	0.0002816	−0.2764060	0.0002444	−0.7554470	0.0047438	−1.0633997	0.0050411	0.1326298	0.0231140
650.00	1.500	−0.4564546	0.0004216	−1.6439866	0.0004054	−0.3268478	0.0003191	−0.8905395	0.0081060	−1.5341516	0.0067478	0.1907071	0.0411992
650.00	2.000	−0.5479908	0.0006694	−2.1573951	0.0003913	−0.3019307	0.0004647	−0.8397671	0.0067531	−2.0900812	0.0092205	0.6743759	0.0579826
650.00	2.500	−0.6018584	0.0009190	−2.6993285	0.0002753	−0.1446229	0.0006192	−0.7379870	0.0038404	−2.8280953	0.0119386	1.4791500	0.0902510
650.00	3.000	−0.5938517	0.0016301	−3.2941645	0.0001609	0.2612336	0.0007044	−0.6816548	0.0021949	−3.7348054	0.0111285	3.1804354	0.1069821
650.00	3.500	−0.4909766	0.0046583	−3.9454853	0.0001152	1.1293554	0.0009333	−0.7303418	0.0014858	−4.7002956	0.0139387	7.3596686	0.1806473
650.00	4.000	−0.2529934	0.0212883	−4.6311789	0.0000874	2.7977817	0.0012152	−0.9070121	0.0020153	−5.4851128	0.0204417	15.1703310	0.2398937
650.00	4.500	0.4165070	0.1833160	−5.2975492	0.0001372	5.7497894	0.0017372	−1.2242195	0.0029193	−5.6790249	0.0310070	28.4046850	0.3675481
650.00	5.000	6.5178416	0.9748886	−5.8564886	0.0002397	10.6476744	0.0024207	−1.6773080	0.0051572	−4.5772436	0.0514476	51.4570615	0.5417032
700.00	0.100	−0.0298265	0.0000555	−0.1048386	0.0000141	−0.0291941	0.0000500	−0.0752639	0.0001211	−0.1040770	0.0003092	0.0034569	0.0019662
700.00	0.500	−0.1392505	0.0001410	−0.5128511	0.0000802	−0.1267642	0.0001268	−0.3459767	0.0009360	−0.4976800	0.0019265	0.0293337	0.0115987
700.00	1.000	−0.2535471	0.0002387	−0.9994444	0.0002061	−0.2021014	0.0002067	−0.5775192	0.0029980	−0.9523751	0.0040631	0.1292202	0.0249744
700.00	1.500	−0.3405877	0.0003772	−1.4714274	0.0002733	−0.2182745	0.0003071	−0.6787575	0.0045246	−1.4041377	0.0066834	0.2857633	0.0358605
700.00	2.000	−0.3964240	0.0004874	−1.9495955	0.0002280	−0.1511224	0.0003750	−0.6657127	0.0041636	−1.9580628	0.0074703	0.7234357	0.0586371
700.00	2.500	−0.4091821	0.0008178	−2.4583582	0.0002016	0.0578848	0.0005219	−0.6185981	0.0026967	−2.6475848	0.0088004	1.5314362	0.0754720

T / K	ρ/ mol·dm^{-3}	A^{r}_{00}	ΔA^{r}_{00}	A^{r}_{10}	ΔA^{r}_{10}	A^{r}_{01}	ΔA^{r}_{01}	A^{r}_{20}	ΔA^{r}_{20}	A^{r}_{11}	ΔA^{r}_{11}	A^{r}_{02}	ΔA^{r}_{02}
700.00	3.000	−0.3619049	0.0015039	−3.0125541	0.0001415	0.5286010	0.0007865	−0.6167834	0.0018813	−3.4695632	0.0092156	3.4907061	0.0971272
700.00	3.500	−0.2104272	0.0044852	−3.6127755	0.0001045	1.4640087	0.0008767	−0.6937150	0.0012900	−4.3170178	0.0127967	7.2779748	0.1496130
700.00	4.000	0.1056538	0.0190467	−4.2365380	0.0000943	3.1851935	0.0012462	−0.8802149	0.0017954	−4.9411372	0.0196814	15.0200226	0.2442517
700.00	4.500	0.7113903	0.1575469	−4.8328165	0.0001356	6.1460804	0.0017869	−1.1978137	0.0030926	−5.0184756	0.0311624	27.9342770	0.3394901
700.00	5.000	6.4779690	0.7097498	−5.3193081	0.0002367	10.9644155	0.0023380	−1.6486766	0.0048878	−3.9431255	0.0463604	49.0805529	0.4749426
800.00	0.100	−0.0172217	0.0000421	−0.0839574	0.0000097	−0.0167086	0.0000381	−0.0515418	0.0000710	−0.0837889	0.0002177	−0.0013744	0.0019145
800.00	0.500	−0.0777522	0.0001130	−0.4137137	0.0000474	−0.0663643	0.0001040	−0.2286105	0.0005361	−0.4073499	0.0012173	0.0073934	0.0092166
800.00	1.000	−0.1323739	0.0002012	−0.8164708	0.0001124	−0.0855773	0.0001783	−0.3784156	0.0014092	−0.7996286	0.0027920	0.1015333	0.0194471
800.00	1.500	−0.1609406	0.0002998	−1.2190986	0.0001481	−0.0426886	0.0002432	−0.4535044	0.0019645	−1.2178906	0.0046504	0.2743203	0.0320016
800.00	2.000	−0.1556142	0.0004521	−1.6364953	0.0001828	0.0941290	0.0003593	−0.4740130	0.0021247	−1.7265173	0.0058155	0.7244869	0.0510142
800.00	2.500	−0.1065208	0.0007474	−2.0825231	0.0001257	0.3893584	0.0005371	−0.4888230	0.0015317	−2.3161975	0.0069197	1.6521737	0.0667181
800.00	3.000	0.0143353	0.0015100	−2.5645824	0.0000951	0.9585195	0.0006517	−0.5314451	0.0010868	−3.0062757	0.0090200	3.5503104	0.1102433
800.00	3.500	0.2475992	0.0041018	−3.0777416	0.0000827	1.9969498	0.0008219	−0.6423173	0.0011336	−3.6453486	0.0107167	7.5691574	0.1280002
800.00	4.000	0.6129371	0.0174412	−3.5990162	0.0000833	3.7895085	0.0010615	−0.8453033	0.0016557	−4.1050489	0.0166298	14.5093371	0.1930978
800.00	4.500	1.2675846	0.1517397	−4.0817838	0.0001273	6.7442972	0.0016419	−1.1541577	0.0030022	−3.9709961	0.0292134	26.6242116	0.3154698
800.00	5.000	8.7166863	0.9414494	−4.4516121	0.0002178	11.4221868	0.0021539	−1.5815274	0.0041040	−2.7722777	0.0397703	46.6573215	0.4140044
900.00	0.100	−0.0082043	0.0000379	−0.0697582	0.0000086	−0.0077168	0.0000343	−0.0377358	0.0000508	−0.0698231	0.0001829	−0.0007915	0.0016972
900.00	0.500	−0.0326281	0.0001047	−0.3460821	0.0000337	−0.0226449	0.0000946	−0.1661944	0.0003129	−0.3431889	0.0009713	0.0327021	0.0079382
900.00	1.000	−0.0436456	0.0001777	−0.6898070	0.0000876	0.0020817	0.0001595	−0.2769826	0.0009720	−0.6926414	0.0022112	0.1013891	0.0177096
900.00	1.500	−0.0280803	0.0002737	−1.0400924	0.0001069	0.0924659	0.0002249	−0.3410615	0.0010683	−1.0702000	0.0030123	0.3153420	0.0289330
900.00	2.000	0.0226362	0.0004439	−1.4078380	0.0001065	0.2847038	0.0003716	−0.3793887	0.0012852	−1.5152975	0.0049661	0.8051929	0.0450609
900.00	2.500	0.1212497	0.0006506	−1.8012918	0.0000889	0.6461693	0.0004614	−0.4135007	0.0008437	−2.0412586	0.0053037	1.6695899	0.0625026
900.00	3.000	0.2937435	0.0011266	−2.2233636	0.0000769	1.2897118	0.0005541	−0.4838950	0.0008658	−2.6089869	0.0071601	3.8403787	0.0792216
900.00	3.500	0.5779098	0.0035577	−2.6663231	0.0000673	2.3972041	0.0009012	−0.6089478	0.0011208	−3.1173096	0.0105342	7.5808694	0.1272849
900.00	4.000	1.0114674	0.0171854	−3.1070456	0.0000687	4.2306082	0.0009950	−0.8177854	0.0017596	−3.4296389	0.0179031	14.0496287	0.1938886
900.00	4.500	1.6163007	0.1650856	−3.5019747	0.0001094	7.1658483	0.0012899	−1.1219803	0.0028966	−3.1973861	0.0289041	25.3595520	0.3064543
900.00	5.000	6.7727690	0.9073186	−3.7845187	0.0001972	11.6974293	0.0019786	−1.5322721	0.0051265	−1.9925357	0.0471239	43.3625616	0.4516755
1000.00	0.100	−0.0014289	0.0000339	−0.0594826	0.0000068	−0.0009052	0.0000308	−0.0290353	0.0000361	−0.0591861	0.0001571	0.0007024	0.0014315
1000.00	0.500	0.0011301	0.0000998	−0.2968512	0.0000275	0.0111157	0.0000920	−0.1282999	0.0002381	−0.2974190	0.0008813	0.0228248	0.0076690
1000.00	1.000	0.0241617	0.0001650	−0.5963172	0.0000609	0.0701493	0.0001474	−0.2175885	0.0005785	−0.6064750	0.0017758	0.0988203	0.0141092
1000.00	1.500	0.0745146	0.0002635	−0.9053072	0.0000723	0.1987372	0.0002354	−0.2763738	0.0007064	−0.9510039	0.0028675	0.3002836	0.0265731
1000.00	2.000	0.1617164	0.0003974	−1.2324918	0.0000759	0.4357673	0.0003130	−0.3194791	0.0007671	−1.3511200	0.0039953	0.8169545	0.0418881
1000.00	2.500	0.3006318	0.0006183	−1.5820765	0.0000755	0.8487967	0.0003795	−0.3705737	0.0007013	−1.8113544	0.0048079	1.7132431	0.0595928
1000.00	3.000	0.5156640	0.0012948	−1.9542853	0.0000630	1.5475766	0.0005377	−0.4510488	0.0007827	−2.2726135	0.0068120	3.8842909	0.0854422

T / K	ρ/ mol·dm^{-3}	A_{00}^{r}	ΔA_{00}^{r}	A_{10}^{r}	ΔA_{10}^{r}	A_{01}^{r}	ΔA_{01}^{r}	A_{20}^{r}	ΔA_{20}^{r}	A_{11}^{r}	ΔA_{11}^{r}	A_{02}^{r}	ΔA_{02}^{r}
1000.00	3.500	0.8430440	0.0033286	−2.3398164	0.0000530	2.7032188	0.0006612	−0.5845921	0.0010426	−2.6805927	0.0100399	7.6994772	0.1180999
1000.00	4.000	1.3165921	0.0142829	−2.7157829	0.0000699	4.5610569	0.0009135	−0.7940028	0.0018292	−2.8750677	0.0178753	13.9655346	0.1910791
1000.00	4.500	2.1466263	0.1190997	−3.0413875	0.0001129	7.4654062	0.0012153	−1.0849081	0.0024735	−2.5099797	0.0250101	24.9294504	0.2712871
1000.00	5.000	5.4310140	0.7131130	−3.2553234	0.0002066	11.8697513	0.0020596	−1.4840018	0.0046681	−1.3067044	0.0425995	41.5326536	0.4082998
1100.00	0.100	0.0039493	0.0000318	−0.0517098	0.0000057	0.0043062	0.0000288	−0.0233231	0.0000273	−0.0518321	0.0001334	−0.0015096	0.0011638
1100.00	0.500	0.0275400	0.0000870	−0.2594164	0.0000207	0.0377393	0.0000788	−0.1039251	0.0001569	−0.2600250	0.0007448	0.0273560	0.0069461
1100.00	1.000	0.0772488	0.0001594	−0.5241282	0.0000482	0.1248472	0.0001460	−0.1783662	0.0004112	−0.5366346	0.0015385	0.1362860	0.0151701
1100.00	1.500	0.1556356	0.0002369	−0.8001934	0.0000610	0.2848335	0.0002114	−0.2331237	0.0005042	−0.8538708	0.0023175	0.3484455	0.0246100
1100.00	2.000	0.2731155	0.0003494	−1.0931119	0.0000626	0.5573277	0.0002819	−0.2814369	0.0005143	−1.2077980	0.0031702	0.8923817	0.0352451
1100.00	2.500	0.4446427	0.0005759	−1.4057550	0.0000628	1.0108988	0.0003793	−0.3404499	0.0005311	−1.6143423	0.0044352	1.8712515	0.0530232
1100.00	3.000	0.6869198	0.0011070	−1.7365993	0.0000487	1.7540939	0.0005414	−0.4307598	0.0007178	−2.0263044	0.0072028	3.8367745	0.0896587
1100.00	3.500	1.0499495	0.0030402	−2.0744880	0.0000476	2.9439186	0.0007051	−0.5706531	0.0009190	−2.3577834	0.0094936	7.3924073	0.1114332
1100.00	4.000	1.5777147	0.0211950	−2.3976761	0.0000866	4.8125596	0.0011294	−0.7744056	0.0020537	−2.4243796	0.0206935	13.8649582	0.2296067
1100.00	4.500	2.1923015	0.2000383	−2.6671577	0.0001636	7.6844807	0.0016784	−1.0625327	0.0035332	−2.0413052	0.0361970	23.6401259	0.3795913
1100.00	5.000	3.0504713	0.5227837	−2.8264234	0.0001970	11.9681014	0.0018050	−1.4430115	0.0041257	−0.7726563	0.0380686	40.0126907	0.3636643
1200.00	0.100	0.0082111	0.0000344	−0.0456419	0.0000051	0.0085315	0.0000320	−0.0192897	0.0000243	−0.0456621	0.0001248	0.0012348	0.0011949
1200.00	0.500	0.0489121	0.0000922	−0.2299007	0.0000173	0.0591361	0.0000868	−0.0871164	0.0001338	−0.2344349	0.0006110	0.0145408	0.0059461
1200.00	1.000	0.1206258	0.0001608	−0.4667140	0.0000383	0.1692489	0.0001463	−0.1520209	0.0002983	−0.4842156	0.0015351	0.1207344	0.0138708
1200.00	1.500	0.2216671	0.0002419	−0.7153530	0.0000508	0.3551158	0.0002141	−0.2037775	0.0004155	−0.7636352	0.0021262	0.3737061	0.0242026
1200.00	2.000	0.3628682	0.0003570	−0.9797415	0.0000545	0.6579063	0.0002956	−0.2560694	0.0004914	−1.0934508	0.0030140	0.8326533	0.0352699
1200.00	2.500	0.5601456	0.0005517	−1.2612613	0.0000492	1.1444130	0.0003643	−0.3197211	0.0005066	−1.4504410	0.0046030	1.8593479	0.0567213
1200.00	3.000	0.8329869	0.0010958	−1.5566827	0.0000472	1.9193685	0.0004714	−0.4150935	0.0005776	−1.8039514	0.0053849	3.8235518	0.0679409
1200.00	3.500	1.2218468	0.0031291	−1.8549104	0.0000515	3.1342022	0.0006232	−0.5553992	0.0009121	−2.0589761	0.0091458	7.3559455	0.1052134
1200.00	4.000	1.7584653	0.0120826	−2.1340079	0.0000737	5.0087803	0.0009515	−0.7583641	0.0013790	−2.0645401	0.0137870	13.4346518	0.1587386
1200.00	4.500	2.5295910	0.0957474	−2.3574994	0.0001114	7.8414129	0.0012283	−1.0366035	0.0024117	−1.6003101	0.0241086	23.1948163	0.2556792
1200.00	5.000	6.3920181	0.5644965	−2.4722328	0.0001702	12.0160818	0.0015683	−1.4040638	0.0040320	−0.3388081	0.0378930	38.3379224	0.3715234

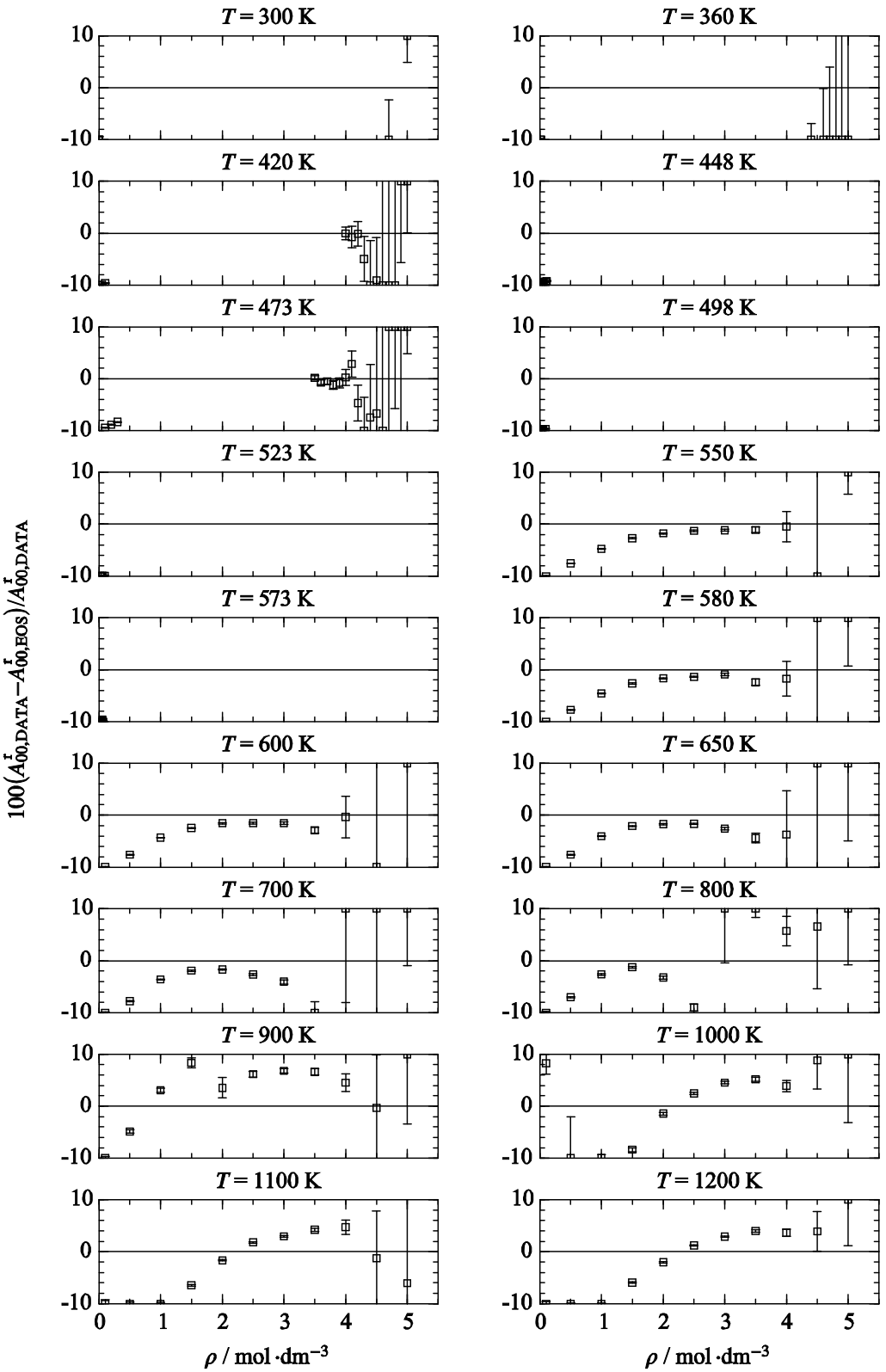

Figure 7. Relative deviations between simulation data and the present equation of state.

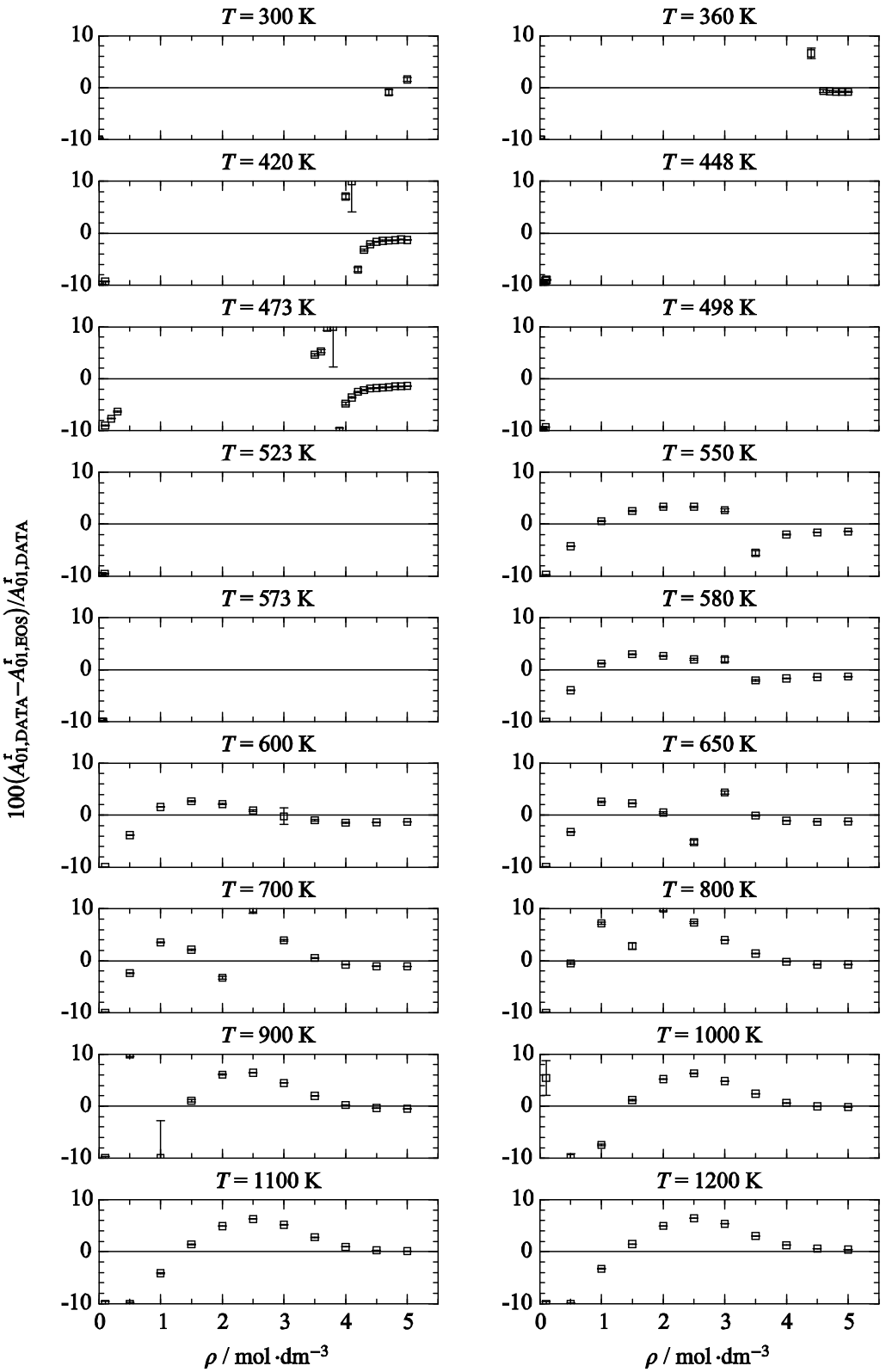

Figure 8. Relative deviations between simulation data and the present equation of state.

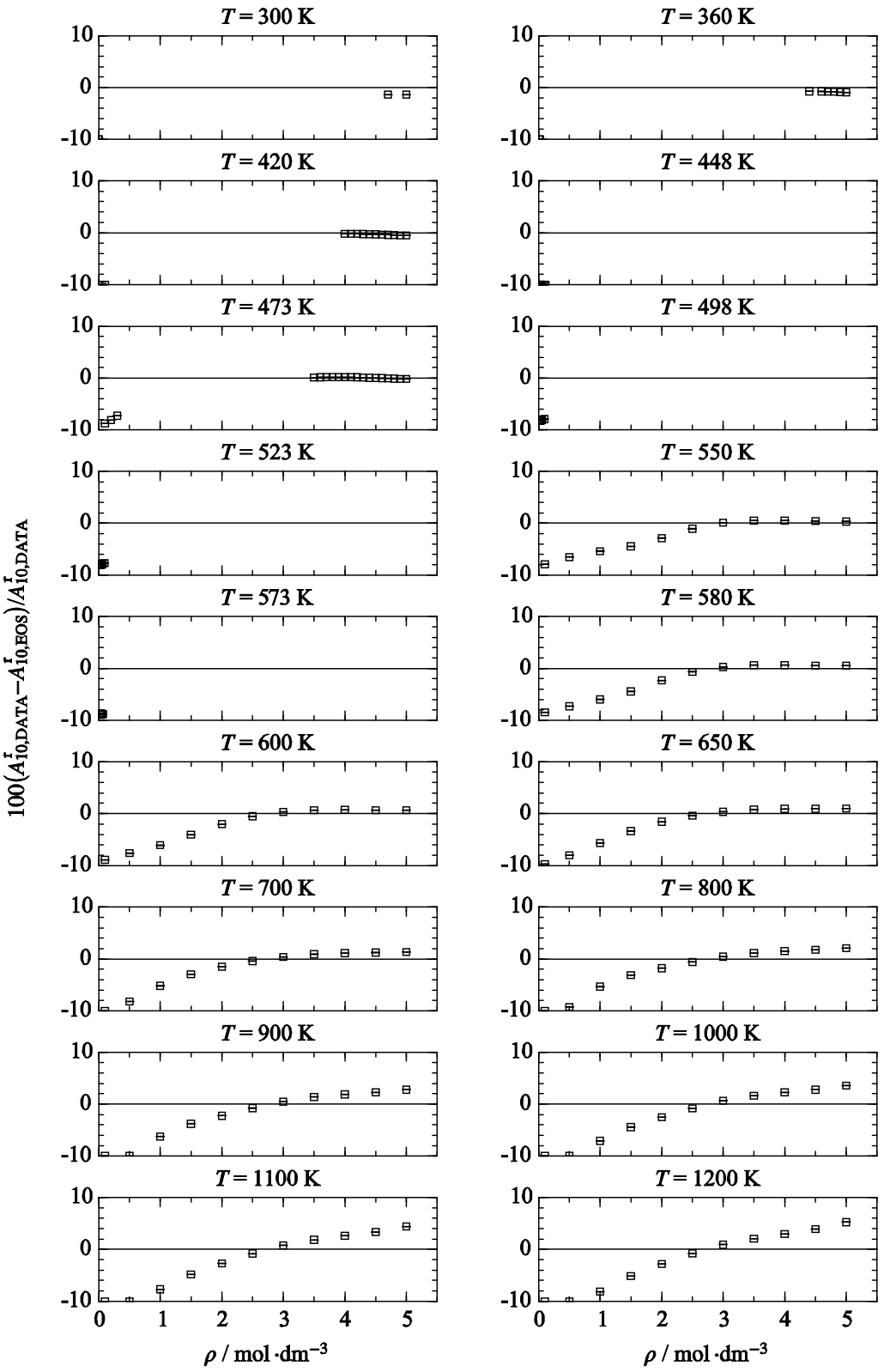

Figure 9. Relative deviations between simulation data and the present equation of state.

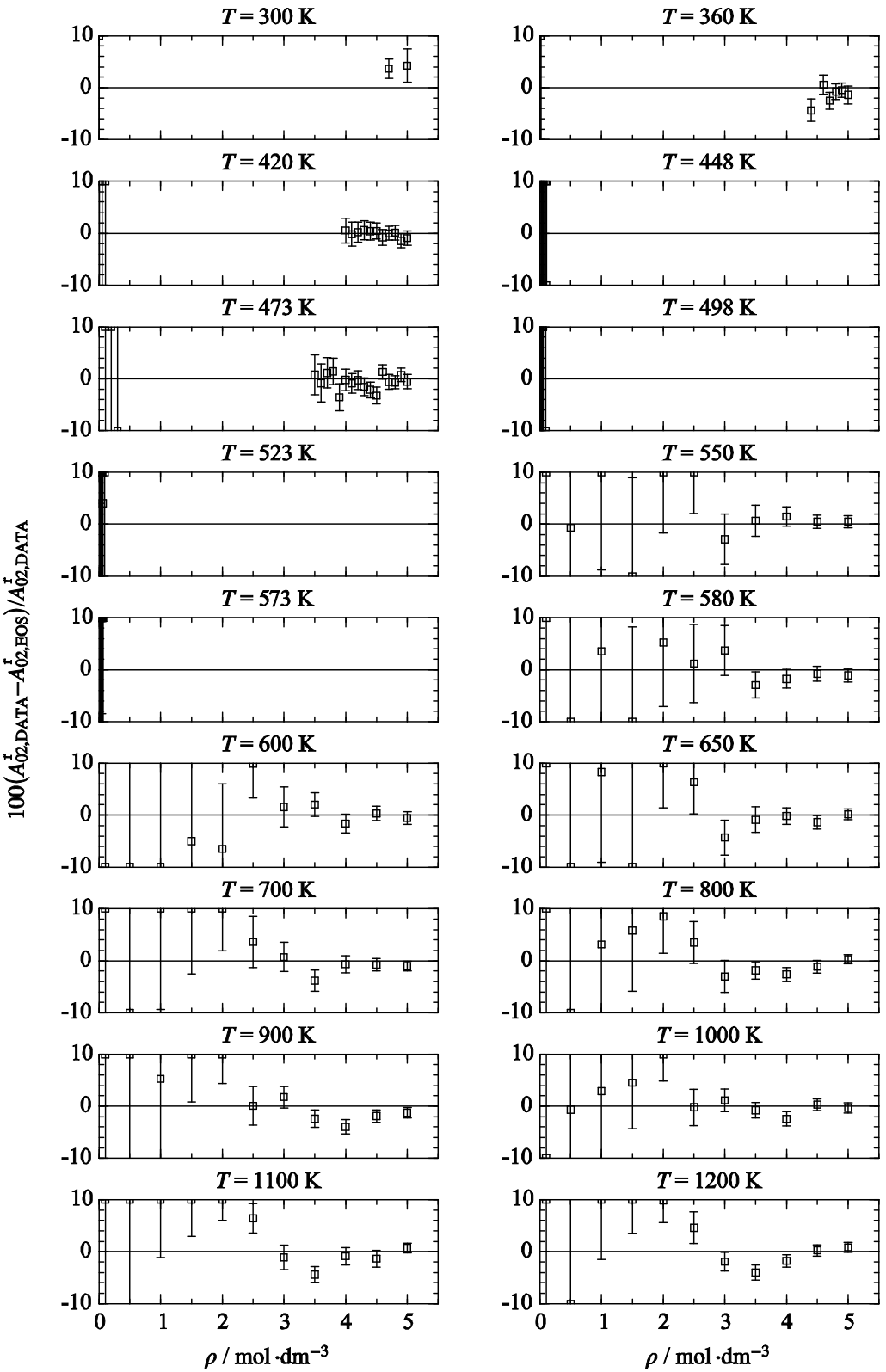

Figure 10. Relative deviations between simulation data and the present equation of state.

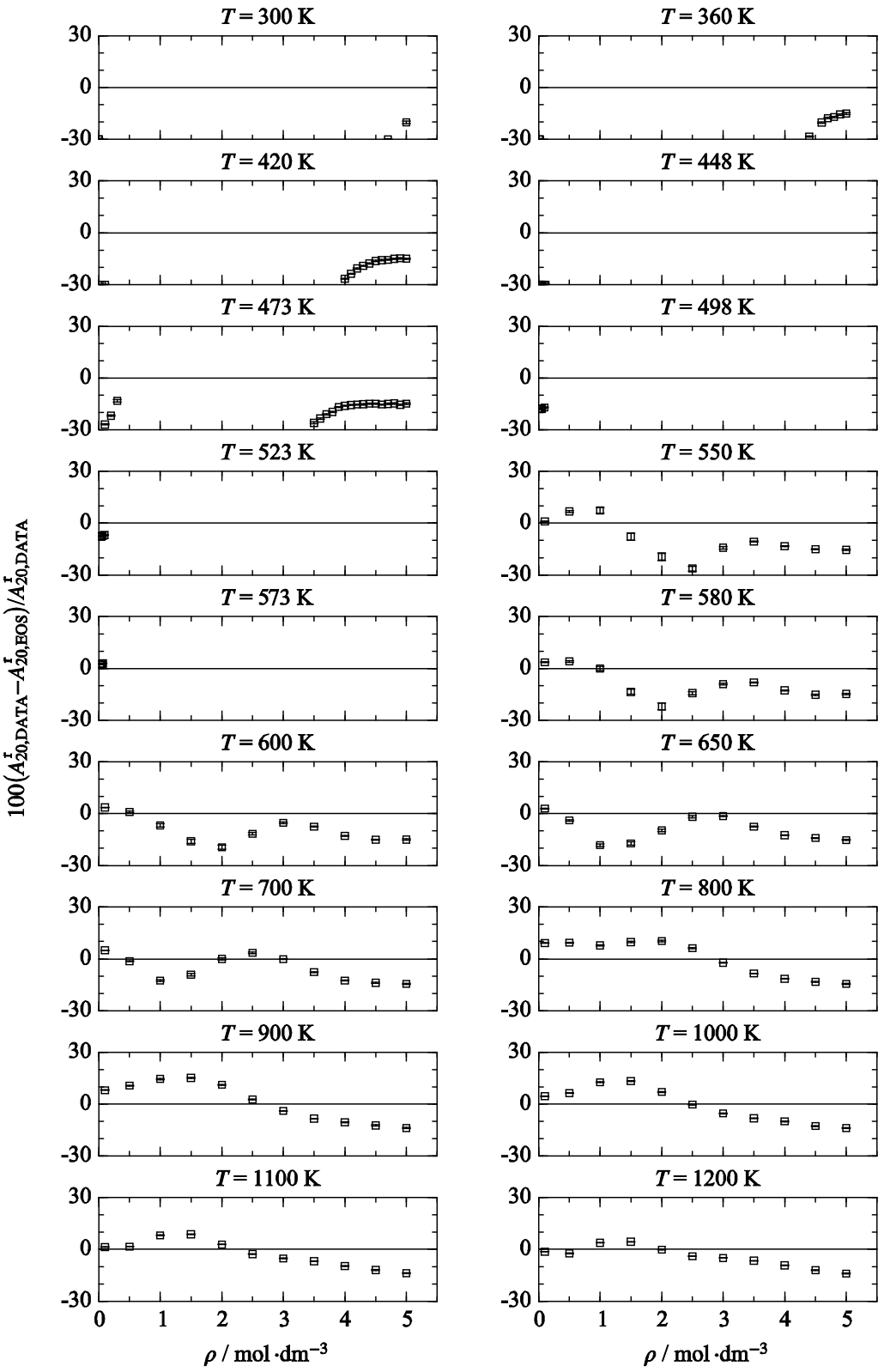

Figure 11. Relative deviations between simulation data and the present equation of state.

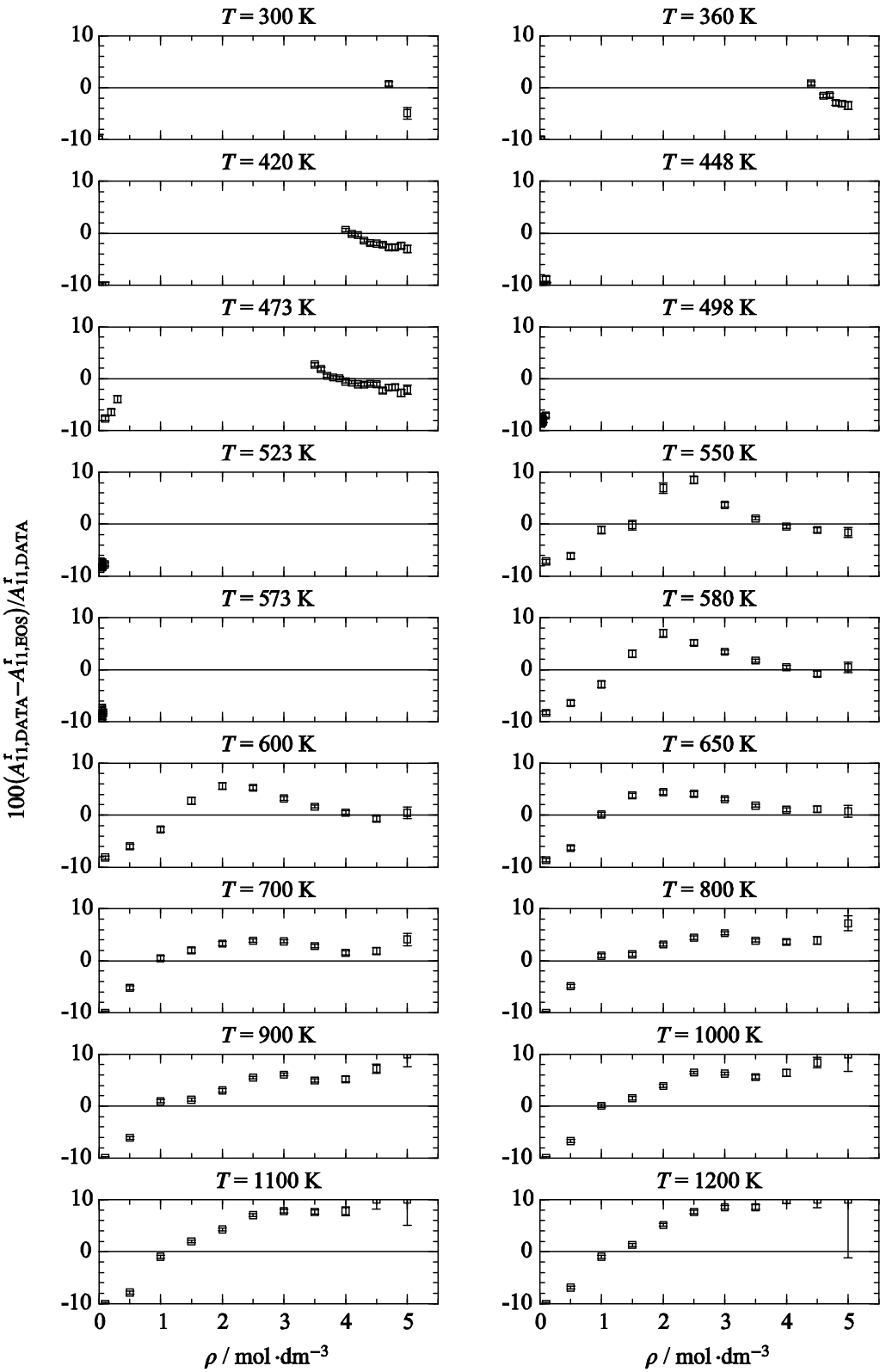

Figure 12. Relative deviations between simulation data and the present equation of state.

References

[1] J. Vrabec and H. Hasse, "Grand equilibrium: vapour-liquid equilibria by a new molecular simulation method," *Mol. Phys.*, vol. 100, pp. 3375–3383, 2002.

[2] B. Widom *J. Chem. Phys.*, vol. 39, pp. 2808–2812, 1963.

[3] J. O. Hirschfelder, C. F. Curtiss, R. B. Bird, and M. G. Mayer, *Molecular theory of gases and liquids*, vol. 26. Wiley New York, 1954.

[4] DDBST, "Dortmunder datenbank, mixture properties, version 6.3.0.384," 2010.

[5] R. Rowley, W. Wilding, J. Oscarson, Y. Yang, N. Zundel, T. Daubert, and R. Danner, *The DIPPR data compilation of pure compound properties.* Design Institute for Physical Properties, AIChE, New York, 2006.

[6] R. Abbas, *Anwendung der Gruppenbeitragszustandsgleichung VTPR für die Analyse von reinen Stoffen und Mischungen als Arbeitsmittel in technischen Kreisprozessen.* PhD thesis, Technische Universität Berlin, Germany, 2011.

[7] D. H. Marcos, D. D. Lindley, K. S. Wilson, W. B. Kay, and H. C. Hershey *J. Chem. Eng. Data*, vol. 56, pp. 5019–5027, 2011.